THE ASTROPHYSICAL JOURNAL, 508:491–517, 1998 December 1

THE EXTRAGALACTIC DISTANCE SCALE KEY PROJECT. XVI. CEPHEID VARIABLES IN AN INNER FIELD OF M101[1]

PETER B. STETSON,[2,3] ABHIJIT SAHA,[4] LAURA FERRARESE,[5] DAYA M. RAWSON,[6] HOLLAND C. FORD,[7]
WENDY L. FREEDMAN,[8] BRAD K. GIBSON,[6] JOHN A. GRAHAM,[9] PAUL HARDING,[10] MINGSHENG HAN,[11]
ROBERT J. HILL[12] JOHN G. HOESSEL,[11] JOHN P. HUCHRA,[13] SHAUN M. G. HUGHES,[14]
GARTH D. ILLINGWORTH,[15] DANIEL D. KELSON,[9] ROBERT C. KENNICUTT, JR.,[10]
BARRY F. MADORE,[5] JEREMY R. MOULD,[6] RANDY L. PHELPS,[8] SHOKO SAKAI,[5]
NANCY A. SILBERMANN,[5] AND ANNE TURNER[10]
Received 1998 April 27; accepted 1998 July 8

ABSTRACT

We report on the identification of 255 candidate variable stars in a field located some 1.′7 from the center of the late-type spiral galaxy M101 = NGC 5457, based on observations made with the Wide Field and Planetary Camera 2 on board the *Hubble Space Telescope*. Photometric measurements in the F555W and F814W filters—analyzed independently with the DAOPHOT/ALLFRAME and DoPHOT software suites—have been transformed to the Johnson V and Kron-Cousins I standard magnitude systems. Periods and intensity-averaged mean magnitudes for 61 carefully selected candidate Cepheid variables with periods in the range 10–48 days indicate a reddening-corrected mean distance modulus $(m - M)_0 = 29.05 \pm 0.14$ (if the true modulus of the Large Magellanic Cloud is 18.50 ± 0.10, and if there is no dependence of the period-luminosity relation on metal abundance); results consistent with this are obtained whether or not the sample is expanded to include a larger fraction of the candidates. Applying a metallicity-dependent correction of $+0.16 \pm 0.10$ mag would increase this estimate to $(m - M)_0 = 29.21 \pm 0.17$ mag.

Subject headings: Cepheids — galaxies: distances and redshifts — galaxies: individual (M101) — galaxies: photometry

1. INTRODUCTION

The goal of the Extragalactic Distance Scale Key Project of the *Hubble Space Telescope* (*HST*) is to measure the value of the local Hubble parameter, H_0, with an accuracy better than 10% (Kennicutt, Freedman, & Mould 1995). Achieving this goal will require the resolution of several outstanding problems with the extragalactic distance scale. The first and most obvious aim of the Key Project is to calibrate numerous secondary distance indicators—such as the Tully-Fisher relation, the planetary nebula luminosity function, the surface-brightness fluctuation technique, and the expanding photospheres method as applied to Type II supernovae—through the detection and measurement of classical Cepheid variable stars in suitable standard galaxies. To exploit these Cepheid variables to the fullest, however, we must also refine our understanding of the intrinsic Cepheid period-luminosity (PL) relation by, for instance, improving our knowledge of the absolute distances of the Magellanic Clouds, and by evaluating any systematic effect of metal abundance on the true PL relation.

The nearby galaxy M101 = NGC 5457 ($\alpha_{2000} = 14^h03^m$, $\delta_{2000} = +54°21'$; $l = 102°$, $b = +60°$) is an excellent place to examine the variation of the Cepheid PL relation with metallicity, following the example of a test using Cepheids in M31 observed from the ground (Freedman & Madore 1990). M101 is a luminous late-type spiral of morphological class Sc(s) I (Sandage & Tammann 1981) or SAB(rs)cd (de Vaucouleurs et al. 1991), with distance estimates ranging between 5 and 8 Mpc; we refer readers to Kelson et al. (1996; hereafter Kel96) for a discussion of the various distance estimates in the literature. As a nearby face-on, grand-design spiral, M101 has been widely used for the study of spiral structure (see, e.g., Elmegreen, Elmegreen, & Montenegro 1992); unfortunately, the low inclination of the galaxy with respect to the plane of the sky makes it of little use as a calibrator of the Tully-Fisher relation. However it does have a large and well-measured metallicity gradient (Shields & Searle 1978; Zaritsky, Elston, & Hill 1990; Scowen, Dufour, & Hester 1992; Kennicutt & Garnett 1996). Direct comparison of the classical Cepheid PL relations in two fields at greatly different distances from the center of M101 can provide a direct measurement of any metallicity-dependent variations in that fundamental relationship.

Accordingly, the *HST* Distance Scale Key Project has observed two fields in M101, the first centered at a galacto-

[1] Based on observations with the NASA/ESA *Hubble Space Telescope*, obtained at the Space Telescope Science Institute, operated by AURA, Inc., under NASA contract No. NAS 5-26555.

[2] Dominion Astrophysical Observatory, Victoria, BC V8X 4M6, Canada.
[3] Guest User, Canadian Astronomy Data Centre, which is operated by the Dominion Astrophysical Observatory for the Canadian National Research Council's Herzberg Institute of Astrophysics.
[4] Space Telescope Science Institute, Baltimore, MD 21218.
[5] IPAC, California Institute of Technology, Pasadena, CA 91125.
[6] Mount Stromlo and Siding Spring Observatories, Institute of Advanced Studies, Australian National University, Weston Creek, ACT 2611, Australia
[7] John Hopkins University and Space Telescope Institute, Baltimore, MD 21218.
[8] Carnegie Observatories, Pasadena, CA 91101.
[9] DTM, Carnegie Institution of Washington, Washington, DC 20015.
[10] Steward Observatories, University of Arizona, Tucson, AZ 85721.
[11] University of Wisconsin, Madison, WI 53706.
[12] Laboratory for Astronomy and Solar Physics, NASA Goddard Space Flight Center, Greenbelt, MD 20771, and Raytheon STX Corporation, Greenbelt, MD 20770.
[13] Harvard Smithsonian Center for Astrophysics, Cambridge, MA 02138.
[14] Royal Greenwich Observatory, Cambridge CB3 0EZ, UK
[15] Lick Observatory, University of California, Santa Cruz, CA 95064.

centric distance of 7.9 and the second at a distance of 1.7. The locations of these fields with respect to M101 as a whole are shown in Figure 1 of Kennicutt et al. (1998; hereafter Ken98). The mean metallicities of the two fields, as determined from measurements of H II regions, differ by a factor of roughly 4, with the metallicity in the outer field approximately equal to that of the Large Magellanic Cloud [specifically, $12 + \log (O/H) = 8.37 \pm 0.15$ in the outer M101 field, $12 + \log (O/H) = 8.5$ for the LMC on the same H II region abundance calibration; Zaritsky, Kennicutt, & Huchra 1994], while the inner-field metal abundance may exceed the solar neighborhood value by a small amount: $12 + \log (O/H) \sim 9.0$ as compared to 8.9 for the solar photosphere. The outer, more metal-poor field of M101 was the subject of an *HST* study based primarily on images from the original Wide Field and Planetary Camera (WF/PC), but included some observations obtained with the second-generation Wide Field and Planetary Camera 2 (WFPC2); the results of this study have been presented by Kel96, who derived a true distance of some 7.4 ± 0.6 Mpc, based upon the period-luminosity relation for 29 Cepheid variables. Since the metallicity of this outer field is virtually the same as that of the LMC, this derived distance is robust against any assumptions about the dependence of the Cepheid PL relation on chemical abundance.

Recently, Kennicutt et al. (1998) have performed a strictly differential comparison of the PL relations of the two fields in M101, employing a photometric calibration based on a small subset of nearly contemporaneous observations obtained with WFPC2 in the F555W and F814W filters to eliminate potential systematic errors arising from uncertainties in the true photometric zero points of early WFPC2 data. (Charge-transfer losses and any change of those losses when the operating temperature of the camera was altered in the early days of WFPC2's mission are still not definitively characterized.) The analysis was based on a subset of very well observed inner-field Cepheids designed to match the period range covered by Cepheids in the shallower outer-field data. The conclusion of that paper was that there may be a small dependence of the observed PL relation on abundance in the sense that, after dereddening, Cepheids in the more metal-rich inner part of M101 appear brighter at a given period than Cepheids in the more metal-poor outer region. (An alternative interpretation is that metal-rich Cepheids are intrinsically redder than metal-poor ones at the same period, and therefore corrections for interstellar extinction are overestimated. These two possible interpretations cannot be distinguished with the available data, but their consequences for the extragalactic distance scale are numerically identical in either case.) The analysis of Ken98 resulted in a metallicity-dependent correction to the dereddened true distance modulus amounting to -0.24 ± 0.16 mag dex^{-1}; this is significant at the 1.5 σ level and could therefore be taken as consistent with no metallicity dependence at all.

Being based as it is on a purely differential comparison of hand-selected samples of inner- and outer-field Cepheids, the Ken98 paper is the most sensitive available test of a radial gradient in the Cepheid PL relation in M101. As mentioned above, in the interests of performing the most strictly differential analysis possible, Ken98 did not analyze the entire sample of Cepheids in the inner M101 field, nor did the paper attempt to use the full body of available data to provide a complete and fundamental photometric calibration for the WFPC2 observations of M101. The present paper is intended to perform that role. Subsequent sections of this paper will describe: § 2, the observations that were obtained for this project, the rectification of the raw digital frames, and the extraction of instrumental photometry for stellar images contained within those frames; § 3, the calibration of the photometry to the Johnson, Kron-Cousins V, I system; § 4, the detection of Cepheid variables and the determination of light-curve parameters; and § 5, the definition of the period-luminosity relations and the estimation of the absolute distance modulus of the M101 inner field. Discussions of independent analyses based upon the DAOPHOT/ALLFRAME and the DoPHOT software suites will be maintained in parallel throughout.

2. OBSERVATIONS AND REDUCTIONS

Observations of the M101 inner field were obtained with the Wide Field Planetary Camera 2 (WFPC2) of the *Hubble Space Telescope* (*HST*) on 11 separate occasions during the 48 day interval from 1994 March 18 to 1994 May 10 (HJD = 2449434.4–2449482.8). On 10 of the visits, individual 1200 s exposures were obtained with the F555W (V) filter, while on the eleventh visit two such exposures were made; on one occasion a single 120 s V-band exposure was also taken. During the same period five F814W (I) exposures were acquired, one of 120 s, one of 1000 s, and three of 1200 s. The inner field of M101 was revisited twice in the 1995 observing season: once a single 1200 s exposure was obtained in F555W, and on the other visit a pair of 500 s F555W exposures was taken. These images form the basis of the present analysis. During the 1994 observing season, two exposures in the F439W (B) filter and two in the F336W (U) were also acquired. These images were included in the ALLFRAME photometric reduction discussed below and they appear in the observation log presented here as Table 1, but they are too shallow to record many of the Cepheids of interest to the immediate study, so they will not be discussed further here. They should, however, be useful for stellar-populations analyses (see, e.g., Bresolin, Kennicutt, & Stetson 1996; Bresolin et al. 1998).

It should be noted that at the majority of the epochs when the inner M101 field was observed, only single exposures were obtained, as opposed to the "cosmic-ray split" pairs of images usually taken when longer total exposure times are required for fainter targets. This characteristic of the data causes some increase in the complexity of the light-curve analysis, when it is necessary to distinguish haphazard anomalies such as cosmic-ray events in the detector from genuine variations in astronomical objects. Six of the visits to the M101 inner field (including the short-exposure V image, but not the short-exposure I image) were made before 1994 April 23, when the operating temperature of the camera was reduced from roughly -77°C to -88°C. All exposures were made in fine guidance lock with the serial clocks off, and the chips were read out through electronics bay 4, yielding a nominal gain of 7 electrons per analog-to-digital converter unit (ADU).

The rectification process applied to these images differs in some small ways from that discussed in the benchmark paper for this series, Hill et al. (1998). In that paper, pipeline-calibrated images were received from the Space Telescope Science Institute and were corrected for sporadically appearing "hot" and "warm" pixels based upon "delta-dark" frames obtained near in time to the program

TABLE 1

LOG OF OBSERVATIONS

Data Set	Filter	Geocentric UT (Start)		HJD (Mid-Exposure)	Exposure (s)
U2780101T	F555W	1994 March 22	22:34	2449434.4434	1200
U2780102T	F814W	1994 March 22	23:52	2449434.4971	1000
U2780103T	F439W	1994 March 23	00:12	2449434.5109	1000
U2780201T	F555W	1994 March 30	13:41	2449442.0731	1200
U2780301T	F555W	1994 April 8	16:47	2449451.2021	1200
U2780302T	F814W	1994 April 8	17:52	2449451.2473	1200
U2780303T	F439W	1994 April 8	18:16	2449451.2640	1200
U2780304T	F336W	1994 April 8	19:28	2449451.3140	1200
U2780305T	F336W	1994 April 8	19:51	2449451.3299	1200
U2780401P	F555W	1994 April 11	05:27	2449453.7299	1200
U2780402T	F555W	1994 April 11	05:41	2449453.7396	120
U2780601T	F555W	1994 April 16	21:19	2449459.3908	1200
U2780701T	F555W	1994 April 20	11:57	2449463.0005	1200
U2780801T	F555W	1994 April 24	17:18	2449467.2233	1200
U2780901T	F555W	1994 April 28	16:13	2449471.1780	1200
U2780A01T	F555W	1994 May 3	16:53	2449476.2056	1200
U2780501T	F555W	1994 May 5	17:21	2449478.2250	1200
U2780502T	F814W	1994 May 5	18:38	2449478.2784	1200
U2780503T	F814W	1994 May 5	18:52	2449478.2881	120
U2780B01T.....	F555W	1994 May 10	03:30	2449482.6477	1200
U2780B02T.....	F814W	1994 May 10	04:46	2449482.7005	1200
U2780C01T	F555W	1994 May 10	08:05	2449482.8387	1200
U2780D01T	F555W	1995 March 22	22:27	2449799.4385	1200
U2MS0301T.....	F555W	1995 April 17	07:42	2449824.8236	500
U2MS0302T.....	F555W	1995 April 17	07:53	2449824.8312	500

observations. In the present study, recalibrated images derived using the best available calibration frames and procedures were requested from the Canadian Astronomy Data Centre (CADC). These differ from the pipeline-calibrated images provided by the institute in that the CADC images have been rectified using the best calibration images available *at the time the request for data was submitted* , rather than the best calibration frames available *at the time the data were obtained* . For observations made very near the beginning of WFPC2's mission, such as the present ones, the distinction could be significant. A careful comparison of the pipeline-calibrated images with the recalibrated images from the CADC reveals that the primary differences are seemingly random changes in the noise (due presumably to improvements in the mean bias, dark, and flat-field images as more calibration frames have been acquired over time), and a more complete mapping of the defective, hot, and warm pixels on each chip in the recalibrated data. The latter change is particularly useful in reducing the confusion between aberrant pixels and variable stars.

The recalibrated images obtained from the CADC were then subjected to a few additional rectification steps, following the standard procedure for papers in the present series. First, from the *HST* Archive, we obtained copies of the flat-field images that had originally been used to normalize our science exposures. Since portions of the digital images that were vignetted by the edges of the fixed pyramid mirror are not so identified in the data-quality files, the V and I flats were converted to a data mask: in each flat-field image, any pixel whose value differed from unity by a factor larger than $2^{1/2}$ (a number chosen arbitrarily) was set to 64; others were set to 0. Then the two images were summed yielding an image containing the value 64 in pixels that were vignetted in one flat-field image, 128 in pixels vignetted in both images, and zero otherwise. This data mask was added to the data-quality arrays provided with the images of the astronomical target, and then these augmented data-quality files were used to mask the science images (viz., if a pixel in the augmented data-quality array contains the value zero, the corresponding pixel in the science image is left alone; if the value in the data-quality file is nonzero, the corresponding pixel in the science image is replaced by an outrageous value that our analysis software will recognize as representing the absence of valid data). While the primary intent is to mask off those regions of each image that are vignetted by the edges of the pyramid mirror, at the same time it masks several small patches of relatively insensitive pixels—perhaps because of dirt on the CCDs or in the optics—particularly on chip WF4. As mentioned above, we noticed that the data-quality files provided by the CADC indicated a significantly higher fraction of defective pixels than those provided by the pipeline; many of these appear to be the hot and warm pixels found in the delta-dark images. Because of these more comprehensive data masks and because the reduction software is designed to be highly robust against defective pixels (such as those generated by cosmic-ray impacts, as well as hot pixels), the obtaining and applying of delta-dark images was judged to be an unnecessary effort and was omitted from the present analysis.

Next, our science exposures were multiplied by a pixel-area map modified slightly from that kindly provided to our group (Jon Holtzman 1998, private communication). The problem is that, because of geometrical distortion in the WFPC2 optics, individual pixels on the CCD do not map to exactly equal areas on the sky. When the flat-field exposures are taken, the pixels that are smaller *in projection* receive fewer photons and, as a result, appear less sensitive. When the science exposures are divided by these flats, the "smaller" pixels near the edges and corners of the chips have their recorded fluxes artificially boosted. Thus, while frames that have been rectified by the standard pipeline flats correctly reproduce the surface brightnesses of astronomical objects, total fluxes integrated over the faces of individual pixels have been distorted. Multiplying the normalized

science images by an array containing the projected pixel areas restores the integrity of flux measurements. Holtzman has normalized his pixel-area maps for the four individual WFPC2 CCDs to the area of pixel (400, 400) on each chip. The nature of the geometric distortion is such that in each case pixel (400, 400) turns out to be among the largest on the chip. We therefore renormalized the maps to the *median* pixel area on each chip, which was approximately 0.985 times the area of pixel (400, 400). This slight adjustment means that the effective readout noise and gain in the science exposures will be unchanged when averaged over the area of each chip, but it does also mean that a small ($\approx$0.016 mag) difference will appear between the calibration zero points appropriate to Holtzman's reductions and those appropriate to ours.

As a last step, all our science images were multiplied by 4.0 and were truncated to short integers. This results in a factor of 2 reduction in the amount of disk space required to store our data (with a further factor of order 2 to be gained when the data are compressed at times when they are not immediately needed), without significant loss of information content: with an effective gain of $1.75e^-$/ADU and an effective readout noise of 4 ADU, our flux measurements are still well sampled. (The use of truncation rather than rounding simply means that the observed sky brightness will be smaller by 0.5 ADU than we would otherwise have observed; this will have no effect on stellar photometry.) This renormalization will lead to a further difference of 2.5 log 4 = 1.505 mag between the zero points that we will employ and those to be found in the literature.

All photometric reductions were based on the fitting of model point-spread functions (PSFs), using both the DAOPHOT/ALLSTAR/ALLFRAME suite of programs (Stetson 1987, 1994; Stetson & Harris 1988), and a modified version of DoPHOT (see Schechter, Mateo, & Saha 1993 for standard DoPHOT; Saha et al. 1994 for the modifications).

2.1. *DAOPHOT and ALLFRAME*

The analysis in the DAOPHOT reduction track followed standard Key Project procedures, which have not previously been spelled out in detail in the literature. First, all the original calibrated images were submitted to the FIND routine, which found primarily the cosmic rays. However, some percentage of the detections represented real stars (and unresolved star clusters, and background galaxies). These were sufficient to estimate the geometric translations and rotations relating the coordinate systems of the various exposures. In particular, we found that the pointing of the first three visits to the M101 inner field differed from the remaining 10 by some 27 and 20 WFC pixels in the two coordinates; superimposed on this was an apparently random epoch-to-epoch pointing dither of some 0.6 WFC pixels, rms. Once these pointing offsets had been measured, it was possible to median average all the exposures obtained with each chip to produce a much deeper image of the field, devoid of significant cosmic rays. Routine DAOPHOT/ALLSTAR procedures were then used to derive a provisional list of stellar-appearing objects, with their estimated positions and rough instrumental magnitudes. This list was then fed, along with the *individual* calibrated science exposures, to the computer program ALLFRAME. This program fits model point-spread functions to suspected stellar objects in all science frames simultaneously; it enforces a self-consistent object list in all of the images of the field while refining the estimates of the objects' positions on the sky, their instrumental magnitudes, and the local underlying sky brightness. ALLFRAME can also make modest adjustments to the provisional geometric transformation equations that relate the various frames' coordinate systems. Because of the relatively large ($\sim$34 WFC pixels) shift between the data from the first three visits and the rest, we found it necessary to use quadratic polynomial geometric transformations to relate the coordinate systems of the various WFC frames, while cubic polynomials were employed in the case of the PC images, where the shifts appeared more than twice as large.

There are few—if any—truly bright, isolated stars in our observations of the inner M101 field. Therefore, for the DAOPHOT-track reductions we adopted point-spread functions based on long-exposure ($>$1200 s) images of the remote globular clusters Palomar 4 and NGC 2419 from the program "Ages for the Outermost Globular Clusters: The Formation of the Galactic Halo" (proposal ID No. 5481, J. E. Hesser, PI), and public-domain images of the *HST* standard field in the globular cluster ω Centauri (proposal ID Nos. 5558, 5565, 5572, 5632, 5646, 5659, and 5663). The actual model PSFs were constructed by the computer program MULTIPSF (Stetson 1993). This program generates a standard DAOPHOT-format hybrid PSF (see, e.g., Stetson 1987; Stetson, Davis, & Crabtree 1990), but, unlike DAOPHOT, it is able to construct that PSF from stellar images distributed over a large number of different digital images. This is exceedingly advantageous for *HST* data, where the PSF is undersampled, variable with position, and usually contaminated by cosmic rays, but is reasonably repeatable from one observation to the next in a given filter. In selecting representative exposures of the ω Cen field, our strategy was to utilize only one or two exposures in each filter from each (approximately monthly) visit of the spacecraft to the target over the period 1994 May 28 to 1994 December 24. The need to get sunlight on its solar panels required that the spacecraft be rolled to a significantly different angle on each of the separate visits. This means that on the revisits the best bright, isolated stars fall at different places on the chip, indeed eventually on different chips. This produces an excellent arrangement of potential PSF stars fully sampling the focal plane in each chip, while not unduly taxing our computer resources. By program design, the available images for each of the two outer-halo globular clusters, Pal 4 and NGC 2419, consisted of a set of eight deep images in each of the V and I filters at a single pointing, with a second set of six shallow images in each filter at a second pointing shifted from the first by approximately 20″ ($\approx$200 WFC pixels, $\approx$430 PC pixels) toward the cluster center, intended to enrich the sample of brighter member stars. These data made up for the small number of independent pointings by possessing a very high surface density of excellent candidate PSF stars.

However, after reflection we decided that there was the possibility that in the much shorter ω Cen images (exposure times $<$60 s), and in the short exposures of Pal 4 and NGC 2419, charge transfer losses might subtly alter the stellar point-spread function: perhaps charge traps that would be filled by sky photons in long exposures would stay armed and steal electrons from the wings of stellar profiles during the readout of shallower exposures. Therefore we eventually decided to drop the ω Cen data and the short exposures of

the other clusters from the definition of our working point-spread functions in V and I. However, the ω Cen data were still relied on for the U and B point-spread functions, since the other two clusters had not been observed in these filters.

By utilizing all available long exposures of Pal 4 and NGC 2419, we were able to construct V- and I-band PSFs from an average of more than 1000 star images spread over some 16 individual frames for each of the WFC chips; a proportionately smaller number of stars (in the same number of frames) was available for the PC chip. The least well determined PSFs are in U and B, being based on some 180 stars distributed over 12 frames, and some 120 stars spread over 15 frames, respectively, for each of the three WFC chips; again a proportionately smaller number of PSF stars was available for the PC. A separate model PSF was generated for each chip/filter combination, and each model was allowed to vary as a quadratic function of position across the face of each chip. Robust statistical techniques were used to eliminate the remaining effects of cosmic rays, and the model PSFs were defined out to a radius of 14 pixels (WFC) and 20 pixels (PC), where they were arbitrarily forced to approach zero surface brightness on an azimuthal average. The net volume of each model PSF was integrated numerically and arbitrarily assigned an instrumental magnitude of $25.00 - \log_{10}$ (volume in ADU). The computer program ALLFRAME (Stetson 1994) was then used to perform profile-fitting photometry for the entire ensemble of M101 images, separately for each chip; this program provides precise relative photometry for each of the stars measured in the field.

Because of small focus variations and residual spacecraft jitter, the relative photometric zero points of the profile-fitting magnitude systems typically differ by a few percent from epoch to epoch. Therefore, during the course of the Key Project we have established the policy of choosing from each of the galaxy fields as many as possible (from a few to several dozen) of the brightest, cleanest, and best-observed stars in each chip. We then digitally subtract the remaining stars from each of the frames and perform concentric-aperture photometry on the chosen stars; 12 apertures with radii ranging from 0.″15 to 0.″50 are used. Because the majority of the Key Project science frames are in the F555W filter, the sample of concentric-aperture measurements in the F814W images is much smaller and could become a significant Achilles' heel for the project. Therefore, a number of deep public-domain—mostly Medium-Deep Survey—images of random fields were requested from the CADC. Stars were identified in these fields and reduced in a fashion identical with the Key Project galaxies and halo globular clusters. All these data sets—all currently available Key Project data, Dr. Hesser's long-exposure data for Pal 4 and NGC 2419 as well as the globular clusters Pal 3 and Eridanus, which were subsequently observed for his team, and the F814W data for the random deep fields—were submitted to a slightly modified version of the program DAOGROW (Stetson 1990). This program defines and fits a one-parameter family of growth curves to the concentric aperture data, with a measure of image-core broadening being allowed to vary from frame to frame. Then for each star it selects the aperture producing the highest signal-to-noise ratio and uses the mean growth curve for that frame to correct that magnitude to the system of the largest aperture (radius = 0.″50; the modification consisted of disabling that line of code that extrapolates the growth curve to twice the radius of the largest aperture—in this case, measurement through the equivalent of a 0.″5 radius aperture was required for comparison to published calibrations). The growth-curve analysis was performed separately for each of the four WFPC2 cameras and separately for V and I, but jointly for all images of all subfields. Comparison between the measured profile-fitting magnitudes and the growth-curve corrected aperture magnitudes particular to a given exposure yields an additive magnitude correction from the relative ALLFRAME magnitudes to an absolute aperture-defined instrumental system; the results of this analysis will be discussed further in § 3.1.

2.2. *DoPHOT*

The DoPHOT analysis did *not* include the 1995 revisits to the M101 inner field. The procedure for DoPHOT-based photometry and discovery of Cepheids has been described in detail elsewhere (Saha et al. 1996). The procedure followed here is identical in almost all respects, and only a brief outline and highlight of the modifications since the above reference need be given here.

The original DoPHOT program (Schechter, Mateo, & Saha 1993) was modified to better adapt it to the peculiar nature of the *HST* WFPC2 data as described in the above reference. The model PSF shape parameters derived from observations of the Leo I dwarf galaxy were used, but the program was allowed to optimize the PSF width and image eccentricity from the data at hand. Star lists were defined independently in the two passbands by running DoPHOT on a deep image made by stacking all the epochs of data after coregistration. The list corresponding to each filter was then applied to each individual epoch, after careful reregistration of the star list coordinates onto the original image(s) at each epoch (to within 0.06 pixels rms) and thereafter holding the positions fixed. The precision of these geometric transformations is limited to the 0.06 pixel level by our ability to centroid on undersampled star images. However, because the transformations can be estimated from very many stars (typically a few hundred), the real accuracy of these transformations is much better. After the images have been registered in this way, DoPHOT then reports fitted magnitudes for all stars, as well as partial-aperture magnitudes for the brighter stars.

There have been some changes to the aperture correction procedure since Saha et al. (1996), and these warrant some description. The DoPHOT variant for WFPC2 now also reports aperture magnitudes for the brighter bona fide stars using circular apertures of radius 5 pixels. The "sky" value is determined such that the aperture growth curve from 6 to 8 pixels radius is as flat as possible. Thus the background is determined very close to the star, in fact within the star's own PSF. Note that this is different from the Holtzman et al. (1995) partial-aperture magnitudes, where their apertures are 0.″5, and sky is taken from a region beyond 3″ from the star. The motivation behind this difference is that in some parts of this M101 field, and certainly in some of the other even more crowded galaxies of this project, the background can change substantially in 3″, because of structure in the ambient galaxy surface brightness. The partial-aperture magnitudes measured in this way do not include all the light from the stars, but they do preserve brightness ratios (or magnitude differences) between stars. The partial-aperture magnitudes reported in this way, hereafter called "PAMs," are determined "in isolation," i.e., after subtrac-

ting all other fitted stars. The PAMs must be tied both to the fitted magnitudes (aperture correction) and to some standard measure of magnitude. We consider each in turn.

Since the PSF fitted is not allowed to vary across the face of the chips, the aperture correction from the fitted magnitudes to the PAMs is not constant. Thus a single offset term is insufficient. A typical field taken in this project does not have a sufficient number of bright uncrowded stars distributed uniformly across the face of the chip to allow us to determine this mapping. We thus break the correction into two parts and map the variation in the aperture correction externally from data more suitable to the problem, but determine an overall offset (which can change because of the exact state of telescope focus, spacecraft jitter, and thermal effects like "breathing") from the particular frame itself. The variation was mapped using data on the Leo I dwarf galaxy. It is well defined by a biquadratic function for each chip and filter. The overall offset terms were calculated from the PAMs and are within a few percent of the value obtained from the Leo I data. This correction, when applied to the fitted magnitudes of all the stars, brings them to the same scale as the PAMs.

It is a tacit assumption that the PSF does not change substantially outside 5 pixels (even on the PC chip) because of small focus changes, jitter, and thermal effects. The extended wings of the PSF on scales larger than 5 pixels are defined (for a given filter and chip) by the micro-roughness of the primary mirror, and by residual aberrations in the telescope optics. Thus we expect the corrections to go from the PAM system to the aperture system of Holtzman et al. to remain unchanged with small drifts in focus, and typical differences in spacecraft jitter and thermal effects. However, we appreciate that this step of the correction is susceptible to changes in the charge transfer behavior of the chips and should be evaluated in data that have similar background and exposure times. For this reason, the Leo I data are unsuitable, since they were taken at a different operating temperature for the chips. The data on the globular clusters NGC 2419 and Pal 4 were deemed better. Both the PAMs and magnitudes in the 0.″5 apertures according to the prescription in Holtzman et al. were evaluated for several stars in these two globular clusters. The differences are ~ 0.02 mag for the WFC chips, and ~ 0.1 mag for the PC chip (where 5 pixels is only $\sim 0.''23$). These differences do not show any dependence on position within the chip and are the same between the Pal 4 and NGC 2419 data to within 0.01 mag, thus supporting our ansatz.

3. CALIBRATION

Calibration of the instrumental magnitudes to the standard Johnson/Kron-Cousins systems was performed separately for the DAOPHOT and DoPHOT reduction tracks, following procedures that have become standard for the present paper series. We would like to warn readers that the photometric behavior of WFPC2 has not yet been definitively characterized. The CCDs in the camera are known to suffer from significant charge-transfer inefficiency, the consequences of which appear to depend on the brightness of a star image and on the diffuse sky brightness in the data frame (see, e.g., Whitmore & Heyer 1997); the charge-transfer inefficiency may also vary with time and may depend upon the wavelength of the light being recorded.

A second procedural problem arises from the difficulty of estimating the total amount of light contained within a 0.″5 aperture centered on a star. This size of synthetic aperture has been adopted as a measurement standard (Holtzman et al. 1995) because it is large enough to be immune to changes in image structure caused by spacecraft jitter and ordinary amounts of defocus caused by secular changes in the spacecraft structure and by "breathing" as a result of, e.g., day/night temperature variations. In any event, we anticipate that the difficulty of correcting our magnitude measurements to 0.″5 synthetic apertures and, in particular, the different ways in which DAOPHOT and DoPHOT undertake those corrections, will be less important for M101 than for the typical galaxy studied in this series of papers: M101 is, relatively speaking, very close and has an abundance of apparently bright, well-isolated stars suitable for estimating aperture corrections. It is quite likely that this fact is largely responsible for the excellent agreement we find between the results of the DAOPHOT and DoPHOT analyses, which—as will be shown below—is considerably better than it has been in some previous papers in the present series.

Both the charge-transfer inefficiency and the correction of profile-fitting photometry to 0.″5 synthetic-aperture photometry remain subjects of active study, both by members of the present team and by others, through reanalysis of archival *HST* imagery and by comparison with ground-based observations. It is to be hoped that considerable improvements in our understanding of both these areas of difficulty will be made soon.

3.1. *DAOPHOT*

ALLFRAME's PSF-fitting method provides relative magnitudes that are individually extremely precise but that are referred to a photometric zero point that can tend to float around a bit (several percent) from one observation to the next, because of profile mismatch caused by modest changes in telescope focus or the history of spacecraft jitter. DAOGROW provides aperture magnitudes that are referred to a rigorously defined zero point but that tend to be rather imprecise (uncertainties of several percent) on a star-to-star basis, primarily because of sky-photon noise in the comparatively large synthetic apertures. The best result is achieved by combining the two: if 0.″5 aperture photometry is available for N stars in a given exposure, then by calculating and applying a weighted mean value of magnitude (aperture) − magnitude (profile fit), one achieves an (F555W, F814W) photometric system as precise as that of the profile fits, and as accurate as several percent divided by root N. For our purposes, these instrumental magnitudes must now be transformed to Johnson V and Kron-Cousins I.

Holtzman et al. (1995) have published just such a transformation. The relevant equations may be expressed

$$V = \mathrm{F555W} + Z_V - 0.052(V-I) + 0.027(V-I)^2 ,$$

$$I = \mathrm{F814W} + Z_I - 0.062(V-I) + 0.025(V-I)^2 .$$

For reasons too trivial to go into here, we find it more convenient to work with equations where the observed quantity is isolated on the left-hand side of the equals sign, while the standard-system quantities are gathered together on the right-hand side:

$$\mathrm{F555W} = V + A_V + 0.052(V-I) - 0.027(V-I)^2 , \quad (1)$$

$$\mathrm{F814W} = I + A_I + 0.062(V-I) - 0.025(V-I)^2 . \quad (2)$$

Furthermore, Holtzman et al. adopted a convention by which the zero of the instrumental magnitude scale corresponds to a count rate of 1 ADU s^{-1}, whereas the DAOPHOT software suite has historically employed the convention that 1 ADU s^{-1} corresponds to instrumental magnitude 25.00. On the face of it, then, $A_V = 25 - Z_V$, and similarly for I. However, recall that before analyzing our images, we multiplied them by 4.0 so that we could convert them to short integers without serious loss of information. We will therefore see 4 times as many of "our" ADUs in a given stellar image, so a given fixed V-magnitude will correspond to a perceived F555W magnitude that is 4 times brighter or, numerically, 1.505 mag *smaller*: $A_V = 25 - Z_V - 1.505$. Next we renormalized the pixel-area map, so that we multiplied our images by a correction that was a factor of 1.015 *larger*; again the perceived instrumental magnitudes become *smaller* by 2.5 log 1.015: $A_V = 25 - Z_V - 1.505 - 0.016$ (in fact, the factor is not exactly 1.015 in all four chips; the true value rather than the representative value of 1.015 is used in the actual numerical analysis). That would be it, except that Holtzman et al. give their zero points as $Z_V + 2.5 \times \log GR_i$, where the GR_i represents the fact that the gains of the two electronics bays on WFPC2 do not differ by a strict factor of 2.0, and the ratio is different for the four chips $i = 1, \ldots, 4$. Holtzman et al. calibrated the gain = $14e^-$/ADU electronics bay, but our observations—like most WFPC2 science data—are taken with the gain = $7e$ ADU^{-1} electronics. Holtzman et al. estimate from the available thermal-vacuum test data that the gain ratios are 1.987, 2.003, 2.006, and 1.955 for chips 1–4, respectively. Taking all these things together, zero points A for our data and our procedure would be equal to 1.007, 1.001, 0.999, and 1.026 mag for the four cameras in V, and 1.893, 1.887, 1.885, and 1.912 mag in I.

Given the importance of the absolute reliability of the calibration to the goals of the Key Project, we were reluctant to adopt these zero points on faith. In particular, in our early experimentation with the data for Pal 4 and NGC 2419, we detected an apparent long- versus-short exposure discrepancy in the zero points of the photometry, in the sense that in long exposures stars were measured a few percent too *bright* in comparison with the short exposures as adjusted by 2.5 times the logarithm of the exposure times. This might be due, for instance, to charge traps in the CCDs that are filled by sky photons in long exposures, but that are free to ingest star-generated photons in short exposures where the sky level is very low. If such an effect is real, the validity of the Holtzman et al. calibration—based entirely on exposures shorter than 300 s of bright targets lying on dark backgrounds—could be in serious question when applied to exposures 4 or more times longer of faint stars superimposed upon a bright galactic disk. In addition to this uncertainty, there is the question of the validity of the corrections from the gain = 14 to the gain = 7 photometric systems: in their paper, Holtzman et al. state that the gain-ratio factors given are "suggested" by the available data. Finally, the Holtzman et al. calibration of WFPC2 F555W and F814W magnitudes to Johnson V and Kron-Cousins I is only partially direct. Part of the process was also the calibration of F555W and F814W as measured by *HST* to data obtained with similar filters and CCD on the ground, and the subsequent comparison of these latter data to Johnson V and Kron-Cousins I. We have no evidence that a serious discrepancy exists between these two halves of the calibration—the authors cite consistency at a level of 2% in V (in the mean, *not* rms) and somewhat worse than this in I. Nevertheless, we felt it would be useful to check on this, and perhaps even to try to improve upon it.

An independent recalibration of the gain = 7 electronics bay by direct comparison with available ground-based photometry in the V, I system (specifically, that realization of the Johnson/Kron-Cousins system that is defined by the published results of Landolt 1992) is currently under way (Stetson 1998). This will be based on an extensive body of data for NGC 2419, as well as smaller data sets for Pal 4 and other globular clusters for which long-exposure WFPC2 images are available. Once this analysis is complete, we intend to recalibrate all of the Key Project observations, and as many of the Cepheid galaxies observed with WF/PC or WFPC2 by other investigative teams as possible. For the purpose of the present paper, however, we will stay consistent with other papers in the current series by adopting the provisional zero points of Hill et al. (1998); these represent a compromise between the zero points of Holtzman et al. (as adjusted according to the considerations outlined above), the results of a preliminary analysis of the NGC 2419 and Pal 4 data, the Gilliland (1994) analysis of WFPC2 images of the open cluster M67, and ground-based imagery of the Key Project target galaxy M100 = NGC 4321. Specifically, the zero points A adopted for the present analysis are 0.969, 0.957, 0.949, and 0.973 mag in V and 1.863, 1.822, 1.851, and 1.878 mag in I for chips 1–4, respectively. In the mean, these differ from Holtzman's zero points by -0.046 ± 0.007 mag (standard deviation of one difference) in V and -0.041 ± 0.016 mag in I. The sense of the difference is that a star of fixed true magnitude produces a smaller instrumental magnitude (i.e., corresponds to a larger number of detected electrons) according to our calibration than according to Holtzman's; conversely, for a fixed number of detected electrons we infer a fainter true standard-system stellar magnitude. The sense of this difference is consistent with the hypothesis that electron traps have consumed a greater proportion of star-generated electrons in Holtzman's short exposures than in our long ones. The net effect is that, by adopting our zero points instead of Holtzman's, we infer Cepheid magnitudes that are ~ 0.05 mag fainter, target galaxies that are $\sim 2\%$ more distant, and a Hubble parameter that is $\sim 2\%$ smaller than would have been the case had we adopted Holtman's calibration verbatim.

In short exposures, at least, the WFPC2 chips appear to require a "ramp" correction to compensate for the likelihood that a stellar image that must be read out through most of the body of the chip (i.e., an image at a high y row number) is likely to lose more photoelectrons to charge traps than an image that fell nearer to the interface between the parallel registers and the serial register (i.e., at a low y row number). For a large range of combinations of star brightness and sky brightness, a correction of order 0.04 mag per 800 pixels appears to be representative (Whitmore & Heyer 1997; our own experiments with WFPC2 images of the globular clusters Palomar 4 and NGC 2419 agree with this assessment). In extreme circumstances, the effect could amount to only 0.02 mag per 800 pixels or less (e.g., for bright stars on a bright background), or as much as 0.10 mag per 800 pixels, or more (for faint stars on a faint background; see Whitmore & Heyer). Given the fact that these effects are still rather poorly characterized (and may in fact

be functions of time), in previous papers in this series we have chosen to adhere as closely as possible to the observed data without encumbering them with a series of conjectural "corrections," in the belief that later it will be simpler to apply corrections once they are well justified than to remove "corrections" that eventually turn out to have been unnecessary. Therefore, as in our previous papers we apply no ramp correction at this time. For a fixed true standard-system magnitude, our instrumental magnitudes will be, on average, some 0.02 mag fainter (larger) than they would have been if a 4% ramp had been applied. We will therefore obtain instrumental magnitudes that are of order 2% fainter, which, with a given fixed set of zero points, yields a galaxy distance that appears 1% larger, and a Hubble parameter that is 1% smaller than we would have found had we applied the ramp. We note that an uncorrected ramp error with a peak-to-peak amplitude of 4% contributes only 1.2%, root-mean-square, to our total error budget. This uncertainty is much smaller than other sources of uncertainty, as will be shown below.

To serve as the means of applying these calibrations to real stars in the images, we hand-picked a sample of non-variable stars to constitute a local standard sequence. All other stars in the field were digitally subtracted from each individual exposure, and the sequence stars were subjected to concentric-aperture photometry in these star-subtracted images, where 12 quasi-circular digital apertures ranging in size from 0″.15 to 0″.50 in radius were employed. Based on these data, for each frame the weighted mean magnitude corrections were determined, relating measurements in each of the eleven smaller apertures to magnitudes as measured in the 0″.50 aperture. For any given star, the signal-to-noise ratio will have a maximum value in one of the apertures, typically one of an intermediate radius: in small apertures the precision is limited because only a fraction of the stellar photons are counted, whereas in large apertures the Poisson statistics of the sky correction become significant. In general, bright stars have a maximum signal-to-noise ratio (S/N) in larger apertures and fainter stars have a maximum S/N in smaller ones (see Stetson 1990 for a more extensive discussion). Furthermore, the mean correction from the magnitude system of an arbitrary aperture to that of the 0″.5 aperture is numerically greater and statistically less certain for the smaller apertures than for the larger ones.

For each star, we (that is, our software) identified the aperture in which the quadrature sum of the uncertainty of the instrumental magnitude itself and the uncertainty of the correction to the system of the 0″.5 aperture was minimized and corrected that measured magnitude to the 0″.5 system. Once this had been done for every sequence star in a frame, we determined the weighted mean additive magnitude correction from the profile-fitting photometry (which is relative to an arbitrary zero point) to the 0″.5 aperture system. Finally, for each sequence star we took as its final measured instrumental magnitude either (1) the optimum aperture magnitude as corrected to 0″.5, or (2) the profile-fitting magnitude as corrected to a 0″.5 aperture, whichever had the smaller combined error of measured magnitude and correction. These instrumental magnitudes were inserted into equations (1) and (2), which were then inverted in a least-squares sense to provide standard-system magnitudes for each star of the local calibrating sequence for each chip. We note here that this analysis was performed for the *long-exposure images only* (exposure time ≥ 500 s), given the possibility that the adopted photometric zero points might not be valid for the shorter exposure times. We looked for systematic differences between magnitudes as measured from images obtained at the warmer operating temperature and those taken at the cooler temperature and did not find any that seemed significant. The calibrating sequences for the four chips in the present study are given in Table 2; the uncertainties quoted are standard errors of the mean magnitudes based on the readout noise and photon noise for each individual measurement, as well as on the actual observation-to-observation repeatability found for each sequence star. The coordinates given in Table 2 will permit interested readers to identify our local standards in images of our field, which may be obtained from one of the *HST* archive sites or from the Key Project home page.[16]

3.2. *DoPHOT*

A detailed description of the DoPHOT analysis has already been given in Saha et al. (1996). Further modifications, particularly in the aperture correction procedure, have been given in this paper in § 2.2. The same renormalization procedures as in the DAOPHOT analysis were applied to the pipeline-calibrated images. With aperture count rates established on the Holtzman et al. (1995) system (§ 2.2 above), their zero points are now adopted. Adjustment must be made for the following.

1. The Holtzman et al. calibrations are given for the $14e^-$/ADU gain setting, while our data are at the $7e^-$/ADU setting. The actual gain ratios derived in Holtzman et al. were used to make the correction.
2. A correction of -0.05 mag is applied to the zero points to account for the long-versus-short zero-point differences and the renormalization of the pixel area maps, following the discussion above; this corresponds to assigning to a star of fixed instrumental magnitude a true magnitude 0.05 mag fainter than would be implied by Holtzman's zero points.

Magnitudes on the F555W and F814W ground system (as defined in Holtzman et al.), are thus obtained. Light-curve and period analysis was done with these ground magnitudes. Mean magnitudes in these two passbands were then converted to $\langle V \rangle$ and $\langle I \rangle$ on the Landolt system using the color transformation equations given by Holtzman et al. (and reproduced in this paper in § 3.1).

4. DETECTION OF CEPHEID VARIABLES

4.1. *The ALLFRAME Search*

The photometric calibration of some 78,000 objects measured in the four WFPC2 chips and the subsequent identification and analysis of candidate variable stars was performed by a computer program written by P. B. S., which performs the following basic tasks.

1. It receives the raw measured f555w and f814w ALLFRAME magnitudes for all stars from all images, and their estimated standard errors (f555w and f814w magnitudes differ from F555W and F814W in that they have not been corrected to the system of 0″.5 aperture measurements). It also receives the list of standard-system magnitudes for the

[16] http://www.ipac.caltech.edu/H0kp/.

TABLE 2

COORDINATES AND MEAN MAGNITUDES FOR LOCAL STANDARDS

Chip	ID	X (pixels)	Y (pixels)	R.A. (J2000)	decl. (J2000)	V (mag)	I (mag)	N_V	N_I
1.....	4947	439.7	276.6	14 03 24.23	+54 21 14.6	21.06 ± 0.01	20.48 ± 0.01	15	4
1.....	6869	292.4	360.7	14 03 23.41	+54 21 17.7	21.18 ± 0.01	20.39 ± 0.12	15	4
1.....	304	310.4	65.7	14 03 24.71	+54 21 25.1	21.38 ± 0.01	21.02 ± 0.02	12	2
1.....	8584	286.0	433.5	14 03 23.08	+54 21 15.9	21.50 ± 0.01	21.04 ± 0.02	15	4
1.....	3242	769.4	201.4	14 03 25.58	+54 21 04.4	21.54 ± 0.01	21.03 ± 0.04	15	4
1.....	12145	190.1	586.2	14 03 22.14	+54 21 15.3	21.70 ± 0.01	21.00 ± 0.17	15	4
1.....	7102	551.8	371.8	14 03 24.17	+54 21 07.8	21.90 ± 0.01	21.12 ± 0.03	15	4
1.....	5771	171.7	311.9	14 03 23.24	+54 21 23.5	22.19 ± 0.01	21.96 ± 0.02	15	4
1.....	9925	644.2	487.7	14 03 23.97	+54 21 01.2	22.22 ± 0.01	21.89 ± 0.05	15	4
1.....	13878	220.7	665.2	14 03 21.90	+54 21 12.0	22.22 ± 0.01	21.00 ± 0.01	15	4
1.....	10603	306.1	517.0	14 03 22.79	+54 21 12.9	22.33 ± 0.01	22.24 ± 0.03	15	4
1.....	9334	815.6	463.0	14 03 24.61	+54 20 55.5	22.47 ± 0.01	22.04 ± 0.03	12	2
1.....	7746	282.3	399.1	14 03 23.22	+54 21 17.0	22.55 ± 0.01	21.98 ± 0.02	15	4
1.....	1103	810.2	104.5	14 03 26.11	+54 21 05.6	22.57 ± 0.01	22.43 ± 0.03	12	2
1.....	7901	602.9	405.2	14 03 24.19	+54 21 05.0	22.62 ± 0.01	21.98 ± 0.13	15	4
1.....	7642	329.1	395.2	14 03 23.38	+54 21 15.4	22.72 ± 0.01	22.67 ± 0.02	15	4
1.....	14228	737.9	682.6	14 03 23.44	+54 20 52.4	22.80 ± 0.01	22.69 ± 0.03	15	4
1.....	9390	763.5	465.7	14 03 24.44	+54 20 57.4	22.82 ± 0.01	21.96 ± 0.02	15	4
1.....	9689	779.4	478.1	14 03 24.44	+54 20 56.5	22.91 ± 0.01	22.06 ± 0.03	15	4
1.....	5694	723.4	308.3	14 03 24.98	+54 21 03.2	22.93 ± 0.01	21.21 ± 0.11	15	4
1.....	7475	265.8	387.7	14 03 23.21	+54 21 17.9	22.94 ± 0.01	22.98 ± 0.03	15	4
1.....	313	633.7	66.2	14 03 25.72	+54 21 13.1	23.02 ± 0.01	22.82 ± 0.19	12	2
1.....	3222	497.2	200.7	14 03 24.73	+54 21 14.5	23.07 ± 0.01	22.73 ± 0.02	15	4
1.....	7936	685.2	406.5	14 03 24.44	+54 21 01.9	23.07 ± 0.01	22.79 ± 0.03	15	4
1.....	7602	684.4	393.5	14 03 24.50	+54 21 02.3	23.14 ± 0.01	23.09 ± 0.04	15	4
1.....	4657	217.6	263.0	14 03 23.59	+54 21 23.1	23.16 ± 0.01	22.92 ± 0.22	15	4
1.....	11479	748.4	556.9	14 03 24.01	+54 20 55.5	23.42 ± 0.01	21.82 ± 0.04	15	4
1.....	5631	158.3	306.0	14 03 23.22	+54 21 24.2	23.45 ± 0.06	20.75 ± 0.03	15	4
2.....	10320	276.0	363.2	14 03 19.49	+54 21 48.9	20.74 ± 0.01	19.87 ± 0.01	15	4
2.....	5298	143.3	194.5	14 03 21.88	+54 21 43.2	21.02 ± 0.01	20.41 ± 0.01	15	4
2.....	21915	687.9	744.1	14 03 13.04	+54 21 55.0	21.12 ± 0.02	20.78 ± 0.03	15	4
2.....	8455	53.8	302.1	14 03 21.97	+54 21 57.3	21.20 ± 0.01	20.99 ± 0.02	12	2
2.....	12587	60.9	438.4	14 03 20.97	+54 22 07.9	21.30 ± 0.01	21.05 ± 0.02	12	2
2.....	14506	550.0	501.3	14 03 15.99	+54 21 43.6	21.49 ± 0.01	21.29 ± 0.02	15	4
2.....	13934	532.4	482.5	14 03 16.29	+54 21 43.2	21.53 ± 0.01	21.70 ± 0.02	15	4
2.....	20221	741.4	686.9	14 03 12.94	+54 21 47.2	21.60 ± 0.01	20.75 ± 0.16	15	4
2.....	4179	474.3	155.3	14 03 19.08	+54 21 20.1	21.61 ± 0.01	20.45 ± 0.01	15	4
2.....	2483	655.5	97.5	14 03 17.79	+54 21 04.5	21.64 ± 0.01	21.07 ± 0.02	15	4
2.....	2510	586.5	98.4	14 03 18.42	+54 21 08.7	21.66 ± 0.01	20.78 ± 0.01	15	4
2.....	16155	533.9	555.1	14 03 15.77	+54 21 49.0	21.70 ± 0.01	20.90 ± 0.03	15	4
2.....	16847	614.4	577.9	14 03 14.87	+54 21 46.0	21.80 ± 0.01	21.61 ± 0.03	14	3
2.....	11787	77.4	411.0	14 03 21.00	+54 22 04.7	21.90 ± 0.01	20.96 ± 0.03	15	4
2.....	1700	588.3	71.4	14 03 18.59	+54 21 06.4	21.96 ± 0.01	21.73 ± 0.03	12	2
2.....	11763	473.0	410.0	14 03 17.34	+54 21 40.9	22.00 ± 0.01	21.85 ± 0.04	15	4
2.....	13471	651.2	467.0	14 03 15.29	+54 21 34.8	22.02 ± 0.01	21.43 ± 0.02	15	4
2.....	3544	550.2	133.6	14 03 18.52	+54 21 13.8	22.05 ± 0.01	22.00 ± 0.04	15	4
2.....	14914	510.5	514.8	14 03 16.27	+54 21 47.1	22.06 ± 0.01	21.66 ± 0.02	15	4
2.....	19659	729.3	668.3	14 03 13.18	+54 21 46.4	22.07 ± 0.01	21.82 ± 0.20	15	4
2.....	10924	377.0	382.1	14 03 18.42	+54 21 44.4	22.08 ± 0.01	21.94 ± 0.07	15	4
2.....	11948	445.0	416.2	14 03 17.55	+54 21 43.0	22.23 ± 0.01	22.19 ± 0.03	15	4
2.....	12667	444.5	440.9	14 03 17.39	+54 21 45.1	22.23 ± 0.02	21.66 ± 0.02	15	4
2.....	19563	210.5	664.9	14 03 18.02	+54 22 17.3	22.26 ± 0.01	21.25 ± 0.03	15	4
2.....	3321	193.6	125.7	14 03 21.89	+54 21 34.6	22.26 ± 0.01	21.32 ± 0.01	15	4
2.....	1901	172.1	78.5	14 03 22.41	+54 21 32.0	22.40 ± 0.01	22.40 ± 0.03	15	4
2.....	3274	178.8	124.6	14 03 22.03	+54 21 35.4	22.42 ± 0.01	22.17 ± 0.03	15	4
2.....	18390	714.9	627.4	14 03 13.59	+54 21 44.0	22.50 ± 0.02	21.79 ± 0.02	15	4
2.....	20956	559.7	711.6	14 03 14.46	+54 22 00.1	22.52 ± 0.01	21.87 ± 0.02	15	4
2.....	3464	651.4	130.7	14 03 17.60	+54 21 07.5	22.57 ± 0.01	22.36 ± 0.04	15	4
2.....	21337	637.4	724.2	14 03 13.65	+54 21 56.5	22.91 ± 0.02	21.19 ± 0.07	15	4
3.....	9867	247.2	430.8	14 03 26.01	+54 22 15.9	20.60 ± 0.01	20.22 ± 0.01	15	4
3.....	1136	291.3	118.4	14 03 22.81	+54 22 00.7	21.61 ± 0.01	20.82 ± 0.02	15	4
3.....	11266	305.6	481.1	14 03 26.08	+54 22 23.7	21.66 ± 0.01	21.44 ± 0.02	15	4
3.....	13407	190.1	550.3	14 03 27.51	+54 22 18.4	21.77 ± 0.01	20.78 ± 0.01	15	4
3.....	16451	611.8	648.4	14 03 25.53	+54 22 58.6	21.85 ± 0.01	21.62 ± 0.02	15	4
3.....	15179	264.9	607.2	14 03 27.53	+54 22 27.9	21.89 ± 0.01	21.03 ± 0.03	15	4
3.....	12256	386.9	513.4	14 03 25.82	+54 22 32.2	21.90 ± 0.01	21.57 ± 0.05	15	4
3.....	13421	465.0	550.6	14 03 25.63	+54 22 40.8	21.95 ± 0.01	21.17 ± 0.02	15	4
3.....	9451	208.4	417.1	14 03 26.15	+54 22 11.9	21.95 ± 0.01	21.06 ± 0.02	15	4
3.....	16903	578.6	664.2	14 03 25.90	+54 22 56.8	22.01 ± 0.01	22.02 ± 0.02	15	4
3.....	9141	190.5	407.1	14 03 26.18	+54 22 09.9	22.01 ± 0.01	22.15 ± 0.02	15	4
3.....	8509	78.2	385.2	14 03 26.75	+54 21 59.4	22.05 ± 0.01	21.27 ± 0.01	15	4
3.....	14226	617.5	575.3	14 03 24.81	+54 22 54.6	22.08 ± 0.01	21.85 ± 0.02	15	4

TABLE 2—*Continued*

Chip	ID	X (pixels)	Y (pixels)	R.A. (J2000)	decl. (J2000)	V (mag)	I (mag)	N_V	N_I
3.....	16192	666.1	640.2	14 03 25.08	+54 23 02.5	22.16 ± 0.01	21.35 ± 0.03	15	4
3.....	8457	183.1	383.4	14 03 26.01	+54 22 07.8	22.19 ± 0.01	21.27 ± 0.06	15	4
3.....	7971	153.4	366.7	14 03 26.06	+54 22 04.4	22.20 ± 0.01	21.40 ± 0.03	15	4
3.....	4084	104.8	226.7	14 03 25.09	+54 21 52.1	22.20 ± 0.01	22.14 ± 0.02	15	4
3.....	16919	779.9	664.6	14 03 24.52	+54 23 13.2	22.26 ± 0.02	22.15 ± 0.03	13	4
3.....	6180	518.3	302.8	14 03 22.96	+54 22 30.2	22.27 ± 0.01	22.10 ± 0.02	15	4
3.....	19029	701.9	743.7	14 03 25.79	+54 23 11.6	22.28 ± 0.01	21.86 ± 0.02	15	4
3.....	17946	569.0	702.1	14 03 26.32	+54 22 58.3	22.31 ± 0.01	22.26 ± 0.02	15	4
3.....	14993	646.2	601.3	14 03 24.85	+54 22 58.5	22.33 ± 0.01	21.82 ± 0.02	15	4
3.....	14867	715.2	597.1	14 03 24.34	+54 23 03.9	22.35 ± 0.01	21.78 ± 0.02	15	4
3.....	16492	570.1	649.7	14 03 25.83	+54 22 55.3	22.43 ± 0.01	21.02 ± 0.02	15	4
3.....	9686	183.8	424.2	14 03 26.39	+54 22 10.3	22.48 ± 0.01	22.30 ± 0.02	15	4
3.....	2540	632.5	171.7	14 03 20.96	+54 22 31.6	22.49 ± 0.01	22.23 ± 0.03	15	4
3.....	1231	772.7	122.3	14 03 19.53	+54 22 40.0	22.60 ± 0.03	21.48 ± 0.08	15	4
3.....	9110	263.0	406.3	14 03 25.68	+54 22 15.7	22.82 ± 0.01	22.49 ± 0.03	15	4
3.....	13304	520.8	547.1	14 03 25.21	+54 22 45.1	22.89 ± 0.02	21.75 ± 0.04	15	4
3.....	15031	634.6	602.6	14 03 24.95	+54 22 57.7	23.02 ± 0.01	21.89 ± 0.06	15	4
4.....	9900	373.6	379.4	14 03 29.30	+54 21 27.8	20.14 ± 0.01	19.48 ± 0.03	15	4
4.....	18293	227.2	667.5	14 03 29.92	+54 20 55.7	20.27 ± 0.01	19.60 ± 0.02	15	4
4.....	20416	453.0	739.6	14 03 32.51	+54 21 03.4	20.96 ± 0.01	20.04 ± 0.01	15	4
4.....	7087	794.2	293.3	14 03 32.62	+54 22 00.1	21.00 ± 0.01	20.64 ± 0.02	15	4
4.....	7510	253.6	307.0	14 03 27.69	+54 21 26.5	21.01 ± 0.02	20.25 ± 0.04	15	4
4.....	18814	306.5	684.7	14 03 30.77	+54 20 59.0	21.04 ± 0.01	20.45 ± 0.03	15	4
4.....	9423	344.7	364.9	14 03 28.93	+54 21 27.3	21.16 ± 0.01	20.85 ± 0.02	15	4
4.....	4620	648.5	216.3	14 03 30.73	+54 21 57.6	21.23 ± 0.01	20.84 ± 0.02	15	4
4.....	13073	255.6	476.4	14 03 28.87	+54 21 12.9	21.38 ± 0.01	20.51 ± 0.01	15	4
4.....	2044	613.5	138.6	14 03 29.87	+54 22 01.8	21.41 ± 0.01	21.06 ± 0.02	15	4
4.....	3888	155.4	193.3	14 03 25.99	+54 21 29.8	21.42 ± 0.01	20.67 ± 0.06	15	4
4.....	16520	209.8	601.4	14 03 29.30	+54 20 60.0	21.44 ± 0.01	21.20 ± 0.03	15	4
4.....	3258	753.4	173.7	14 03 31.42	+54 22 07.4	21.45 ± 0.01	20.41 ± 0.02	15	4
4.....	17627	521.2	643.7	14 03 32.49	+54 21 15.2	21.46 ± 0.01	21.02 ± 0.01	15	4
4.....	8122	716.4	326.0	14 03 32.12	+54 21 52.8	21.46 ± 0.01	20.67 ± 0.02	15	4
4.....	21031	210.9	761.4	14 03 30.41	+54 20 47.1	21.47 ± 0.01	21.16 ± 0.02	15	4
4.....	13236	235.5	482.1	14 03 28.72	+54 21 11.2	21.50 ± 0.01	21.39 ± 0.02	15	4
4.....	11591	556.9	429.4	14 03 31.35	+54 21 34.8	21.52 ± 0.01	20.87 ± 0.01	15	4
4.....	4883	477.7	223.9	14 03 29.20	+54 21 46.7	21.53 ± 0.02	20.76 ± 0.02	15	4
4.....	2174	707.7	142.9	14 03 30.78	+54 22 07.1	21.59 ± 0.01	21.34 ± 0.02	15	4
4.....	7940	322.1	320.3	14 03 28.41	+54 21 29.5	21.66 ± 0.01	21.10 ± 0.02	15	4
4.....	2819	621.3	161.3	14 03 30.10	+54 22 00.4	21.70 ± 0.01	21.60 ± 0.03	15	4
4.....	15710	359.3	571.4	14 03 30.49	+54 21 11.4	21.72 ± 0.01	21.52 ± 0.03	15	4
4.....	6929	253.0	288.4	14 03 27.55	+54 21 28.0	21.72 ± 0.02	20.73 ± 0.01	15	4
4.....	8378	475.7	334.4	14 03 29.94	+54 21 37.6	21.74 ± 0.01	20.99 ± 0.01	15	4
4.....	19633	226.5	712.9	14 03 30.22	+54 20 51.9	21.76 ± 0.01	21.03 ± 0.03	15	4
4.....	2144	197.2	141.9	14 03 26.03	+54 21 36.5	21.77 ± 0.01	21.25 ± 0.01	15	4
4.....	19461	258.3	707.2	14 03 30.48	+54 20 54.3	21.81 ± 0.01	21.56 ± 0.02	15	4
4.....	21907	488.8	794.1	14 03 33.22	+54 21 01.1	21.84 ± 0.01	19.03 ± 0.01	15	4
4.....	11976	345.8	441.3	14 03 29.47	+54 21 21.1	21.85 ± 0.01	21.47 ± 0.03	15	4
4.....	2417	474.6	150.4	14 03 28.66	+54 21 52.5	21.86 ± 0.01	21.83 ± 0.02	15	4
4.....	7432	284.4	304.1	14 03 27.95	+54 21 28.6	21.87 ± 0.01	21.63 ± 0.02	15	4
4.....	13738	205.1	500.7	14 03 28.57	+54 21 07.9	21.92 ± 0.01	21.76 ± 0.02	15	4
4.....	5106	406.9	230.4	14 03 28.59	+54 21 41.9	21.95 ± 0.01	20.77 ± 0.01	15	4
4.....	8691	311.2	343.1	14 03 28.47	+54 21 27.0	22.00 ± 0.01	22.04 ± 0.03	15	4
4.....	2176	773.3	143.0	14 03 31.39	+54 22 11.0	22.03 ± 0.01	21.49 ± 0.02	15	4
4.....	14923	490.6	542.8	14 03 31.51	+54 21 21.6	22.07 ± 0.01	21.87 ± 0.05	15	4
4.....	3148	199.9	170.0	14 03 26.25	+54 21 34.4	22.10 ± 0.01	21.93 ± 0.02	15	4
4.....	18946	149.9	689.4	14 03 29.35	+54 20 49.2	22.14 ± 0.01	21.64 ± 0.02	15	4
4.....	8210	131.5	329.2	14 03 26.71	+54 21 17.4	22.20 ± 0.01	21.81 ± 0.02	15	4
4.....	17273	369.7	630.3	14 03 30.99	+54 21 07.2	22.22 ± 0.01	21.75 ± 0.02	15	4
4.....	5427	422.3	240.3	14 03 28.80	+54 21 42.1	22.22 ± 0.02	21.63 ± 0.04	15	4
4.....	786	586.7	97.6	14 03 29.34	+54 22 03.5	22.33 ± 0.01	21.61 ± 0.06	15	4
4.....	9905	121.8	379.6	14 03 26.96	+54 21 12.7	22.39 ± 0.01	21.81 ± 0.03	15	4
4.....	16241	628.9	590.9	14 03 33.12	+54 21 26.0	22.47 ± 0.03	21.87 ± 0.02	15	4
4.....	21736	108.2	787.0	14 03 29.63	+54 20 38.8	22.55 ± 0.01	21.89 ± 0.12	13	4
4.....	1055	635.6	107.5	14 03 29.87	+54 22 05.7	22.55 ± 0.01	22.03 ± 0.02	15	4
4.....	10095	426.7	385.2	14 03 29.83	+54 21 30.6	22.58 ± 0.02	21.76 ± 0.14	15	4
4.....	19737	196.6	716.5	14 03 29.97	+54 20 49.8	22.68 ± 0.01	20.86 ± 0.02	15	4
4.....	20709	183.5	750.5	14 03 30.08	+54 20 46.3	22.68 ± 0.01	21.88 ± 0.03	15	4

NOTE.—Units of right ascension are hours, minutes, and seconds, and units of declination are degrees, arcminutes, and arcseconds.

local standard-sequence stars in each chip, as defined in § 3.1 above. Note that these standard sequences have been defined by measurements in long-exposure images only, using the appropriate long-exposure zero points.

2. Taking these latter magnitudes as representing truth (albeit with an uncertainty associated with each datum), for each frame it determines by least squares the zero point required to place the profile-fitting magnitudes directly onto the Johnson/Kron-Cousins V, I photometric system via equations (1) and (2). Because the effective photometric zero point of each individual exposure is redetermined from stars of "known" standard-system magnitudes, it is now possible to include the images with shorter exposure times in the analysis. Furthermore, since for each frame the system of profile-fitting magnitudes with its floating zero point is now referred directly to the standard system via standard stars contained within the image itself, aperture corrections are irrelevant at this stage; concern with the corrections to 0.″5 apertures are limited to the definition of the local standard sequences (Table 2), as described in § 3.1. This helps to compartmentalize the error budget: *all* the individual images are referred to precisely the same photometric system with an accuracy of order $\sigma_{\rm internal}$:

$$\sigma^2_{\rm internal} = \frac{\sigma^2_{\rm profile}}{N_{\rm loc.stand.}} ,$$

where $\sigma_{\rm profile}$ is the precision of an individual profile-fitting magnitude measurement ($\sim$0.02–0.03 mag, standard deviation) and $N_{\rm loc.stand.}$ is the number of local standards on the chip, typically a couple dozen. Thus, all exposures are related to some self-consistent magnitude system with an internal precision of order a few times 0.001 mag. That magnitude system is equal to Landolt's Johnson/Kron-Cousins magnitude system with an external accuracy determined by the precision of the raw photometry ($\sigma_{\rm profile}$), the number of local standards on the chip ($N_{\rm loc.stand.}$), the precision of the mean aperture correction for a typical frame ($\sigma_{\rm ap.corr.} \sim 0.01$ mag), the number of exposures ($N_{\rm obs} \sim 15$ for F555W, $\sim$4 for F814W), and the uncertainty of the fundamental zero-points and charge-transfer efficiency corrections ($\sigma_{\rm ZP}$)—we estimate that these quantities are currently known only at a level of order 0.03 mag. Thus,

$$\sigma^2_{\rm external} = \left[\frac{\sigma^2_{\rm profile}}{N_{\rm loc.stand.}} + \sigma^2_{\rm ap.corr.} \right] \Big/ N_{\rm obs} + \sigma^2_{\rm ZP} .$$

The former uncertainty ($\sigma_{\rm internal} \sim$ a few times 0.001 mag) represents the amount by which the indeterminacy of individual frames' effective zero points will amplify the light-curve scatter of any given Cepheid; the latter ($\sigma_{\rm external} \sim$ 0.03 mag) represents the contribution of the external photometric uncertainty to the standard error of the derived distance modulus.

3. Using Holtzman's color terms and the individual frame zero points derived in step (2), our software then inverts the calibration equations to solve for the best—in a robust least-squares sense—mean V- and I- band magnitudes for each star, under the assumption that it is not variable.

4. Next, it examines the fitting residuals of each star and computes a variability index as proposed by Welch & Stetson (1993; hereafter WS93), and as subsequently modified by Stetson (1996) specifically to deal with data sets like the present one.

5. If a star has been measured in enough frames, is bright enough, and has a large enough value of the variability index (see below), the data for the star are subjected to a "string-length" analysis to search for candidate periods.

6. For each of the likely candidate periods, a robust least-squares fit to a template Cepheid light curve is performed, the form of the template light curve being a unique function of the assumed period.

7. The best-fitting light curve is identified and reported; plausible alternative light-curve solutions are also reported, but we have never yet encountered a case in which one of these alternate solutions appeared preferable to the best-fitting one. The reader is referred to Stetson (1996) for more complete details of how this is done, but there are a few points worth making here.

First, the WS93 technique is at its most effective when it is applied to data that were taken in pairs or clusters, such as when a field is observed through different filters in rapid succession each time the target is visited, or when cosmic-ray–split pairs of exposures are made with WFPC2. The criterion of variability is then the degree of correlation among the photometric residuals from independent exposures that were taken close together in time: a strong correlation is good evidence of temporal variation, while a lack of correlation or even an anticorrelation of the residuals indicates that observational errors or corrupt data dominate over any intrinsic variability. In the present study, the WS93 technique cannot be used to full advantage because few pairs of exposures were taken—most epochs are represented by only a single image. Under these circumstances, the modified WS93 technique degenerates to what is basically a robust ratio of external to internal error. As a result, a star unfortunate enough to be damaged by cosmic-ray events or detector blemishes on several occasions is likely to be flagged as a candidate variable.

Second, the template-fitting technique employs all the F555W and F814W data available for a given candidate variable to solve for only five unknowns: the period of variation, the V-band amplitude of the variation, the epoch of zero phase, and the mean V- and I-band magnitudes. All other details of the light curve, such as the ratio of the amplitude of variation in I to that in V, and the amplitudes and phases of the low-order Fourier components, have been shown to be well-determined, essentially unique functions of period. Since the F555W data are far more numerous and tend to be of slightly higher quality, and since the amplitude of Cepheid variability is larger in V than in I, the F555W data dominate the determination of the first four unknowns, while the F814W data are left essentially free to determine the mean I-band magnitude alone. Once these five parameters have been determined, the Cepheid light curve is completely specified in both filters and at all phases. The instantaneous magnitudes appropriate to each phase can be calculated, and the full light curve can be converted to flux units and numerically integrated to yield an intensity-averaged magnitude, without any need for ad hoc phase weighting to derive a representative mean magnitude from individual observed magnitudes that may not uniformly sample the variation.

Third is a minor point but a nice one. Since the light curve has been fully specified in each photometric bandpass, the color of the Cepheid at each epoch can also be predicted. Thus, even when the F555W and F814W data were not

taken contemporaneously, each individual observation of a Cepheid can be transformed from the instrumental to the standard system on the basis of the star's predicted instantaneous true color, rather than from some time-averaged ($\langle V\rangle - \langle I\rangle$) or $\langle V-I\rangle$ color.

In the present study a star was initially selected as a candidate variable if it met the following criteria: (1) the star must have been measured in at least 10 F555W images (of 16 possible: 15 long-exposure and one short-exposure) *and* at least three F814W images (of five possible: four long and one short); (2) the star must have a final estimated mean V-band magnitude brighter than 27.0; and (3) the star must have a modified WS93 index ≥ 0.600. On the four chips, a total of some 49,000 stars met the first two criteria; Figure 1 shows them plotted with the WS93 index as a function of magnitude. Among these stars the variability index averaged -0.169 ± 0.251 (standard deviation), so in this case a detection limit of $+0.6$ corresponds to a one-sided 3.06 σ confidence level—about 11 false detections per 10,000 stars if the index behaves as a normal distribution.

The fact that the mean WS93 index comes out negative is in itself interesting. For nonpaired observations, the WS93 index boils down essentially to the ratio of external error to internal error *minus* 1. For this index to tend negative, therefore, the external error must typically be *smaller* than the internal error. This can be understood as a consequence of undersampling and PSF variation: the internal error is estimated, in part, on the basis of the quality of the profile fits. In an undersampled profile, it is hard to predict correctly the specific brightness that should occur in any one pixel, and if the shape of the profile varies spatially in ways not faithfully reproduced by the model PSF, this will make the fits look bad, too. However, the least-squares process has the mathematical property of tending to conserve the total flux in the image: even if the model does not correctly predict the exact distribution of the light in a given star's profile, the best-fitting model PSF will still tend to have the same total volume as the actual profile. A direct comparison of the frame-to-frame repeatability of our derived photometry indicates that the actual random errors of the magnitudes are only about 75% as large as the errors reported by the photometry program. In what follows, however, we will retain the more pessimistic error estimates provided by the algorithm to err on the side of conservatism.

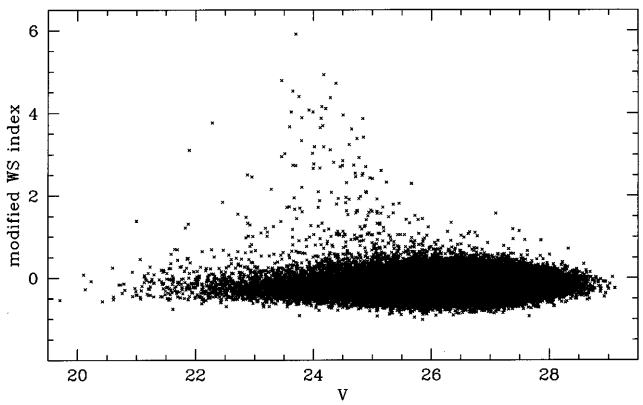

FIG. 1.—Modified WS93 variability index vs. magnitude for approximately 49,000 stars observed in the M101 inner field. Large positive values of the index indicate a significant likelihood that the star is a physical variable.

To further refine the sample of high-quality variability detections, two further impersonal criteria were imposed. First, the template-light-curve fitting algorithm must have been able to identify coherent variation with a period in excess of 2.0 days. Second, the candidate must not be unduly crowded by neighbors. This discrimination was made as follows: each of the 78,000-odd stars appearing in the complete star list was assumed to have a light distribution that could be characterized by a Moffat function (Moffat 1969) with exponent $\beta = 2$, and a full width at half-maximum of 1.0 pixels in the case of WFC, 1.5 pixels in the case of PC. At the centroid of each star, the surface brightness produced by the profiles of all other stars in the image was summed and compared to the central surface brightness of that star itself. If the candidate's central surface brightness exceeded the sum of all other stars in the frame by a factor of 10 or greater, it was retained; if the ratio was smaller than 10, it was discarded. On the face of it, this cutoff appears arbitrary, but at least it is completely objective, and it has been calibrated to agree with the average of many subjective decisions that "this star is too crowded" or "this star is acceptable." A total of 279 candidate variable stars passed all these tests.

Automatic techniques are still not fully reliable in identifying and rejecting (1) stars whose images are corrupted by the wings or diffraction spikes of stars that are so much brighter that they were saturated in the images and thus never made it into the official star list for the field, (2) "stars" that are really barely resolved star clusters or background galaxies, (3) stars closely associated with dust lanes, H II regions, or other nonstellar features in the underlying sky flux, (4) the roughly 11 constant stars per 10,000 expected to have been selected simply by their occupying the >3.06 σ tail of the distribution of the variability index, or (5) stars whose photometry may be dubious for any of various other reasons. Similarly, it is not yet safe to put absolute trust in light curves derived by blind template fits. However, the relatively large sample of 279 machine-selected variable candidates obtained here offers an opportunity to examine the importance of subjective selection criteria, the extent of the bias that they may impose on derived results, and the possibility of someday devising strictly impersonal criteria that can be used to produce the largest possible, cleanest possible sample of uncontaminated Cepheids in an objective and repeatable fashion.

Accordingly, we subjected both the images and the template light-curve fits to visual examination and assigned subjective quality scores. Four of the authors of this paper (S. S., N. A. S., P. B. S., and A. T.) examined all variable candidates both in median-averaged images of each subfield and in median averages of images from which all detected stars had been subtracted. Based on the appearance of the stellar image itself and on the appearance of the fitting residuals after digital subtraction of all detected stars, each author assigned each candidate a score on a scale of 1 ("clean, well-exposed, isolated star") to 4 ("not a star") with two levels of "not so good" in between. Five authors (the four above plus J. A. G.) then graded the fitted light curves on a scale of 1 ("well-sampled Cepheid light curve") to 4 ("not a variable star") with two degrees of "I'm not so sure I'd include this in a PL relation" in between. We found that the individual graders' scores deviated from the mean with a standard deviation typically of order 0.3 (on a scale of 1.0–4.0). The four image quality scores were averaged, the

five light-curve quality scores were averaged, and then the mean image quality scores were averaged with the mean light-curve quality scores to yield a single unidimensional quality index, ranging from 1.0 ("perfect") to 4.0 ("worthless"). After these tests had been performed, and after the list of ALLFRAME variable candidates had been examined in the DoPHOT photometric results (see below), we decided to increase the minimum acceptable value of the WS93 variability index from 0.600 to 0.640 (the smallest value of this index among the variables confirmed by the DoPHOT photometry was 0.641), resulting in a final ALLFRAME sample of 255 variable candidates; these stars are listed in Table 3, and our averaged numerical quality scores are presented in Table 4. A table containing individual-epoch magnitudes for all these stars, finding charts, light curves, and the actual median-averaged images derived for the four chips are available in a publicly accessible archive connected to the Key Project home page;[17] they may also be obtained in hard copy or electronic form upon request directed to the first author of the present paper.

ALLFRAME and the subsequent processing yield a few objective indices of image quality: for each stellar image measured, ALLFRAME returns the index "chi," which is the ratio of the observed standard deviation of the pixel residuals from the profile fit to that expected from the readout and photon noise, and "sharp," which is a measure of the degree to which positive and negative fitting residuals are concentrated toward or away from the center of the profile: a positive value of "sharp" indicates a preponderance of positive residuals at large radii and suggests that the detection is more radially extended than the standard stellar profile, i.e., that it may be a marginally resolved star cluster or background galaxy. Finally, recall that in the postprocessing we estimated the degree to which each candidate Cepheid was isolated from its neighbors via the ratio of surface brightnesses. On close examination, none of these indices showed any particular correlation with the subjective image quality scores assigned by the authors.

The postprocessing software similarly provides at least three numerical indices of the significance of the perceived variability: the modified WS93 index itself, the amplitude of the fitted light curve (very small amplitudes and unphysically large amplitudes suggesting the perceived variation betrays some quirk of the data rather than true astronomical variability), and the ratio of the quality of the second-best fitted light curve to that of the best (this being based on a combination of the rms magnitude residual, the fitted amplitude, and the fraction of observations that had to be discarded to make a clean-looking light curve), the presumption being that if the variation is real, then phasing the data on the true period will produce a light curve far better than phasing them on some other random period, whereas if the variation is spurious, several different periods may produce light curves of comparable unattractiveness. Of these, only the modified WS93 index shows any signs of correlation with the subjective light-curve scores assigned by the authors (Fig. 2). As one might naively expect, stars with the largest value of the WS93 index are the most likely to produce light curves inspiring the highest level of confidence. The converse is less true: a small value of the WS93 index is no guarantee that the variable candidate will appear to be of low quality (although it does increase the chances).

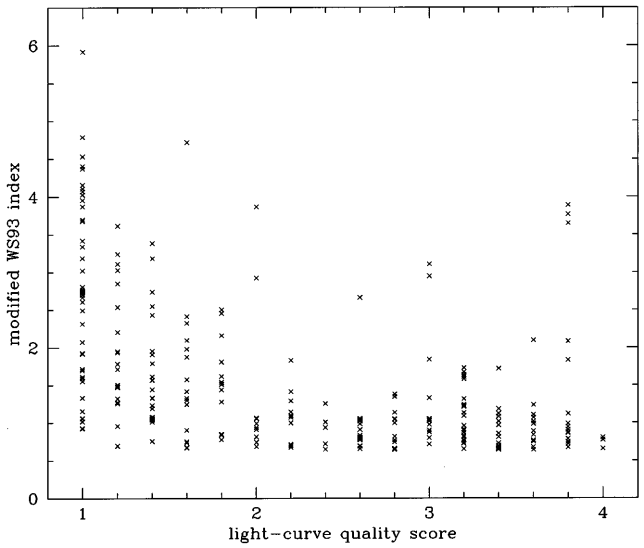

FIG. 2.—Correlation between the subjective light-curve quality scores assigned visually by five team members and the modified WS93 index for 255 variable stars in the inner field of M101.

4.2. *The DoPHOT Search*

The ALLFRAME analysis produced a list of variable candidates that was, by design, as inclusive as possible, in the expectation that the large sample would enable us to experiment with automatic, impersonal methods of distinguishing good Cepheids from poor ones. The authors who performed the DoPHOT analysis, on the other hand, continued their previous practice (see, e.g., Saha et al. 1994; Ferrarese et al. 1998) of being highly selective in assembling their sample of Cepheids, carefully examining all candidates and retaining only those that exhibit minimal blending and unimpeachable light curves. Accordingly, the DoPHOT analysis resulted in the independent selection of only 70 variable candidates, of which 67 are in common with the 279 originally identified in the DAOPHOT/ALLFRAME analysis. Two of the other three DoPHOT candidates were actually flagged as variables in the ALLFRAME data, but they marginally failed the objective crowding test: their surface brightnesses at their centroid positions were only 2.33 mag and 2.39 mag above the sums of the surface brightnesses of all other stars (the cutoff was at 2.50 mag). The remaining DoPHOT candidate was not flagged as a possible variable in the ALLFRAME data; its modified WS93 index was only -0.018, compared to a mean of -0.169 and a standard deviation of 0.251. Thus, according to the ALLFRAME data, at least, this star would be considered a variable only at about a 0.6 σ confidence level (roughly 2700 false detections per 10,000 stars).

After the ALLFRAME analysis had been performed, the 279 original ALLFRAME candidates were ex post facto reexamined in the DoPHOT photometry lists, and it was concluded that 26 additional candidates also had acceptable light curves in the DoPHOT data. This yielded a total of 93 uncrowded Cepheids common to the two data sets; these stars are compared in Table 5. The periods all agree within the range $-0.05 \leq \Delta \log (P) \leq +0.05$ (recall that the DoPHOT analysis did not include the 1995 revisits),

[17] http://www.ipac.caltech.edu/H0kp/.

TABLE 3

VARIABLE COORDINATES, PERIODS, AND MEAN MAGNITUDES

ID	Chip	X (pixels)	Y (pixels)	R.A. (J2000)	decl. (J2000)	P (days)	$\langle V \rangle$ (mag)	$\langle I \rangle$ (mag)
1	1	831.0	73.6	14 03 26.31	54 21 05.6	8.69 ± 0.01	25.18 ± 0.04	24.31 ± 0.09
2	1	648.2	104.6	14 03 25.61	54 21 11.5	35.07 ± 0.06	24.94 ± 0.03	23.40 ± 0.04
3	1	719.7	109.1	14 03 25.81	54 21 08.8	16.27 ± 0.02	24.23 ± 0.02	23.39 ± 0.03
4	1	508.8	173.3	14 03 24.88	54 21 14.8	53.72 ± 2.13	25.84 ± 0.05	24.30 ± 0.05
5	1	808.9	192.8	14 03 25.74	54 21 03.2	20.72 ± 0.04	24.19 ± 0.02	23.45 ± 0.05
6	1	697.1	239.9	14 03 25.19	54 21 06.0	19.25 ± 0.02	24.12 ± 0.01	23.26 ± 0.03
7	1	447.3	265.1	14 03 24.30	54 21 14.6	92.89 ± 0.90	24.83 ± 0.02	21.59 ± 0.01
8	1	307.1	293.0	14 03 23.74	54 21 19.0	14.89 ± 0.02	24.83 ± 0.03	23.87 ± 0.06
9	1	158.3	306.0	14 03 23.22	54 21 24.2	4.14 ± 0.00	23.70 ± 0.03	20.80 ± 0.03
10.....	1	252.1	307.6	14 03 23.51	54 21 20.6	22.89 ± 0.11	24.45 ± 0.03	23.43 ± 0.05
11.....	1	142.0	316.1	14 03 23.13	54 21 24.5	41.97 ± 0.95	23.47 ± 0.02	22.46 ± 0.03
12.....	1	393.3	328.1	14 03 23.86	54 21 14.9	12.73 ± 0.01	25.12 ± 0.02	24.15 ± 0.04
13.....	1	423.3	359.1	14 03 23.83	54 21 12.9	2.20 ± 0.00	24.06 ± 0.03	23.84 ± 0.06
14.....	1	792.8	434.5	14 03 24.66	54 20 57.2	2.06 ± 0.00	22.91 ± 0.01	22.86 ± 0.03
15.....	1	659.2	440.6	14 03 24.22	54 21 01.9	37.43 ± 0.21	24.76 ± 0.02	24.68 ± 0.08
16.....	1	624.1	459.1	14 03 24.03	54 21 02.7	2.95 ± 0.00	24.40 ± 0.02	24.68 ± 0.10
17.....	1	233.5	474.3	14 03 22.74	54 21 16.8	4.53 ± 0.00	23.91 ± 0.01	23.82 ± 0.06
18.....	1	692.4	512.1	14 03 24.02	54 20 58.8	21.87 ± 0.08	24.74 ± 0.02	23.59 ± 0.04
19.....	1	316.9	715.1	14 03 21.99	54 21 07.1	57.20 ± 0.62	26.16 ± 0.06	24.34 ± 0.06
20.....	2	239.0	57.5	14 03 21.93	54 21 26.3	3.32 ± 0.00	23.41 ± 0.01	23.58 ± 0.05
21.....	2	692.0	76.3	14 03 17.60	54 21 00.6	7.88 ± 0.01	22.95 ± 0.01	22.48 ± 0.02
22.....	2	459.3	98.4	14 03 19.61	54 21 16.4	97.28 ± 1.63	25.99 ± 0.06	24.25 ± 0.11
23.....	2	244.1	104.4	14 03 21.56	54 21 29.8	17.05 ± 0.03	24.00 ± 0.02	23.05 ± 0.03
24.....	2	742.9	128.0	14 03 16.77	54 21 01.7	3.31 ± 0.00	26.25 ± 0.10	23.47 ± 0.07
25.....	2	536.7	132.4	14 03 18.65	54 21 14.5	17.37 ± 0.02	24.57 ± 0.03	23.54 ± 0.04
26.....	2	428.9	152.0	14 03 19.52	54 21 22.6	14.36 ± 0.02	24.96 ± 0.02	24.14 ± 0.05
27.....	2	745.7	163.0	14 03 16.50	54 21 04.4	3.87 ± 0.01	25.49 ± 0.05	23.57 ± 0.07
28.....	2	481.3	166.0	14 03 18.94	54 21 20.6	2.18 ± 0.00	25.53 ± 0.05	24.58 ± 0.08
29.....	2	83.5	170.3	14 03 22.60	54 21 44.8	89.51 ± 0.51	26.12 ± 0.06	23.92 ± 0.05
30.....	2	394.0	172.8	14 03 19.70	54 21 26.3	15.03 ± 0.02	24.91 ± 0.02	24.06 ± 0.05
31.....	2	587.6	190.1	14 03 17.78	54 21 16.1	6.76 ± 0.02	25.98 ± 0.05	24.89 ± 0.15
32.....	2	315.4	198.2	14 03 20.26	54 21 33.1	7.55 ± 0.02	26.13 ± 0.05	24.59 ± 0.08
33.....	2	572.1	201.4	14 03 17.85	54 21 18.0	34.76 ± 0.28	23.87 ± 0.02	22.93 ± 0.03
34.....	2	309.1	210.8	14 03 20.23	54 21 34.5	2.81 ± 0.00	23.82 ± 0.04	23.81 ± 0.07
35.....	2	683.7	211.5	14 03 16.74	54 21 12.1	6.26 ± 0.02	22.76 ± 0.01	20.62 ± 0.02
36.....	2	166.8	218.7	14 03 21.50	54 21 43.7	28.85 ± 0.06	24.55 ± 0.02	23.51 ± 0.05
37.....	2	605.6	223.5	14 03 17.39	54 21 17.7	93.43 ± 0.65	21.79 ± 0.03	20.73 ± 0.03
38.....	2	315.6	236.0	14 03 19.99	54 21 36.2	12.20 ± 0.01	23.82 ± 0.02	23.64 ± 0.08
39.....	2	487.3	276.9	14 03 18.12	54 21 29.2	2.46 ± 0.00	24.99 ± 0.04	24.86 ± 0.18
40.....	2	176.3	294.6	14 03 20.89	54 21 49.3	65.21 ± 3.39	26.31 ± 0.07	24.24 ± 0.05
41.....	2	156.2	302.8	14 03 21.02	54 21 51.2	32.83 ± 0.13	23.63 ± 0.01	22.62 ± 0.02
42.....	2	460.4	306.6	14 03 18.16	54 21 33.2	54.40 ± 0.37	24.53 ± 0.01	23.73 ± 0.04
43.....	2	364.5	316.2	14 03 18.99	54 21 39.8	9.55 ± 0.01	24.96 ± 0.03	24.65 ± 0.12
44.....	2	461.8	317.8	14 03 18.07	54 21 34.0	6.71 ± 0.01	24.91 ± 0.08	24.15 ± 0.25
45.....	2	435.3	328.3	14 03 18.25	54 21 36.5	9.65 ± 0.01	24.84 ± 0.02	24.26 ± 0.07
46.....	2	112.7	354.9	14 03 21.06	54 21 58.0	11.75 ± 0.01	25.63 ± 0.03	24.39 ± 0.04
47.....	2	346.0	357.7	14 03 18.87	54 21 44.2	4.09 ± 0.01	23.15 ± 0.02	20.71 ± 0.03
48.....	2	309.0	359.3	14 03 19.21	54 21 46.6	7.64 ± 0.01	24.18 ± 0.04	24.09 ± 0.09
49.....	2	377.0	382.1	14 03 18.42	54 21 44.4	84.15 ± 0.43	22.07 ± 0.01	21.96 ± 0.01
50.....	2	148.9	391.4	14 03 20.47	54 21 58.8	14.30 ± 0.02	25.11 ± 0.03	24.25 ± 0.05
51.....	2	395.8	392.0	14 03 18.18	54 21 44.0	12.97 ± 0.01	24.89 ± 0.03	23.96 ± 0.05
52.....	2	554.5	434.1	14 03 16.41	54 21 37.9	17.85 ± 0.02	24.96 ± 0.03	23.78 ± 0.04
53.....	2	589.4	435.2	14 03 16.08	54 21 35.9	5.57 ± 0.00	25.04 ± 0.04	24.06 ± 0.11
54.....	2	444.5	440.9	14 03 17.39	54 21 45.1	4.18 ± 0.04	22.29 ± 0.03	21.69 ± 0.03
55.....	2	675.2	441.5	14 03 15.24	54 21 31.3	2.21 ± 0.00	26.26 ± 0.09	24.33 ± 0.11
56.....	2	482.2	443.2	14 03 17.02	54 21 43.0	12.12 ± 0.01	23.58 ± 0.02	20.90 ± 0.02
57.....	2	155.9	450.3	14 03 20.00	54 22 03.2	10.48 ± 0.04	23.66 ± 0.01	23.71 ± 0.04
58.....	2	439.0	502.5	14 03 17.02	54 21 50.4	7.61 ± 0.02	26.10 ± 0.07	24.57 ± 0.09
59.....	2	533.9	555.1	14 03 15.77	54 21 49.0	84.13 ± 1.31	21.71 ± 0.01	20.90 ± 0.01
60.....	2	108.4	597.3	14 03 19.43	54 22 18.0	18.68 ± 0.05	25.18 ± 0.03	23.93 ± 0.05
61.....	2	597.9	610.7	14 03 14.80	54 21 49.6	8.73 ± 0.02	24.84 ± 0.09	23.91 ± 0.20
62.....	2	695.5	630.9	14 03 13.75	54 21 45.4	5.42 ± 0.00	24.18 ± 0.01	23.46 ± 0.04
63.....	2	433.0	641.7	14 03 16.11	54 22 02.1	11.95 ± 0.01	25.16 ± 0.04	24.54 ± 0.09
64.....	2	206.5	669.8	14 03 18.02	54 22 18.0	101.0 ± 0.86	23.21 ± 0.01	21.92 ± 0.02
65.....	2	482.7	697.0	14 03 15.27	54 22 03.6	7.66 ± 0.01	24.30 ± 0.05	24.19 ± 0.17
66.....	2	637.4	724.2	14 03 13.65	54 21 56.5	99.17 ± 0.80	22.94 ± 0.01	21.26 ± 0.02
67.....	2	248.0	726.6	14 03 17.25	54 22 20.1	3.32 ± 0.00	23.66 ± 0.02	22.74 ± 0.03
68.....	2	714.6	746.5	14 03 12.78	54 21 53.6	13.52 ± 0.07	24.97 ± 0.03	23.94 ± 0.08
69.....	2	704.3	765.5	14 03 12.74	54 21 55.8	3.88 ± 0.01	24.45 ± 0.02	23.95 ± 0.06
70.....	2	225.7	775.7	14 03 17.12	54 22 25.4	6.14 ± 0.04	25.21 ± 0.04	23.93 ± 0.05
71.....	2	453.4	779.7	14 03 14.97	54 22 12.0	3.31 ± 0.05	23.83 ± 0.19	23.49 ± 0.24
72.....	2	296.7	780.5	14 03 16.42	54 22 21.5	4.28 ± 0.02	23.80 ± 0.12	23.12 ± 0.16

TABLE 3—*Continued*

ID	Chip	X (pixels)	Y (pixels)	R.A. (J2000)	decl. (J2000)	P (days)	$\langle V \rangle$ (mag)	$\langle I \rangle$ (mag)
73	3	196.6	107.1	14 03 23.35	54 21 52.3	17.92 ± 0.01	24.31 ± 0.02	23.45 ± 0.04
74	3	421.6	163.8	14 03 22.33	54 22 14.0	42.37 ± 0.14	24.13 ± 0.02	22.81 ± 0.03
75	3	649.8	176.7	14 03 20.88	54 22 33.3	2.49 ± 0.00	26.15 ± 0.09	24.62 ± 0.11
76	3	680.9	218.9	14 03 21.06	54 22 38.4	2.41 ± 0.00	24.50 ± 0.04	24.67 ± 0.10
77	3	547.0	218.9	14 03 21.98	54 22 27.5	26.21 ± 0.06	24.37 ± 0.01	23.38 ± 0.02
78	3	753.2	225.7	14 03 20.63	54 22 44.6	20.27 ± 0.02	24.25 ± 0.02	23.40 ± 0.03
79	3	379.4	232.2	14 03 23.26	54 22 14.7	6.09 ± 0.01	25.77 ± 0.05	25.31 ± 0.17
80	3	406.4	232.5	14 03 23.08	54 22 16.9	104.4 ± 7.94	26.15 ± 0.06	24.04 ± 0.06
81	3	533.3	264.6	14 03 22.50	54 22 29.1	13.60 ± 0.01	24.62 ± 0.02	23.88 ± 0.03
82	3	580.6	296.5	14 03 22.47	54 22 34.9	7.46 ± 0.01	26.51 ± 0.07	24.50 ± 0.05
83	3	705.1	334.8	14 03 21.97	54 22 47.3	2.77 ± 0.00	25.36 ± 0.03	22.35 ± 0.01
84	3	90.7	359.1	14 03 26.42	54 21 58.9	37.99 ± 0.12	22.77 ± 0.02	22.11 ± 0.03
85	3	180.2	407.7	14 03 26.26	54 22 09.1	7.45 ± 0.01	24.85 ± 0.03	24.09 ± 0.06
86	3	250.9	414.0	14 03 25.83	54 22 15.2	2.23 ± 0.00	25.65 ± 0.05	22.29 ± 0.03
87	3	307.9	435.8	14 03 25.64	54 22 21.1	3.22 ± 0.00	24.43 ± 0.03	23.59 ± 0.05
88	3	728.8	451.2	14 03 22.89	54 22 56.2	16.56 ± 0.02	24.59 ± 0.02	23.59 ± 0.03
89	3	518.9	460.2	14 03 24.42	54 22 39.7	2.25 ± 0.00	25.81 ± 0.05	22.23 ± 0.03
90	3	641.1	467.3	14 03 23.64	54 22 50.1	4.16 ± 0.01	24.22 ± 0.03	22.38 ± 0.04
91	3	389.2	471.9	14 03 25.42	54 22 29.9	13.35 ± 0.03	25.81 ± 0.05	24.72 ± 0.07
92	3	314.0	473.7	14 03 25.95	54 22 23.9	2.51 ± 0.00	24.95 ± 0.03	22.18 ± 0.02
93	3	671.2	473.7	14 03 23.50	54 22 52.9	6.40 ± 0.00	25.23 ± 0.03	24.56 ± 0.08
94	3	558.1	488.2	14 03 24.41	54 22 44.6	17.46 ± 0.01	24.27 ± 0.01	23.34 ± 0.02
95	3	417.5	488.5	14 03 25.38	54 22 33.2	15.20 ± 0.02	25.50 ± 0.03	24.09 ± 0.05
96	3	549.5	491.2	14 03 24.50	54 22 44.1	2.28 ± 0.00	22.01 ± 0.02	21.11 ± 0.03
97	3	436.1	492.5	14 03 25.29	54 22 34.9	14.99 ± 0.05	24.76 ± 0.02	23.97 ± 0.03
98	3	545.3	494.2	14 03 24.55	54 22 43.9	6.94 ± 0.00	17.98 ± 0.02	17.02 ± 0.04
99	3	633.3	522.1	14 03 24.21	54 22 52.7	3.79 ± 0.00	26.13 ± 0.05	24.20 ± 0.05
100.....	3	232.6	524.1	14 03 26.98	54 22 20.3	10.83 ± 0.01	24.90 ± 0.02	24.12 ± 0.05
101.....	3	83.2	533.1	14 03 28.09	54 22 08.7	21.08 ± 0.04	24.46 ± 0.02	23.67 ± 0.04
102.....	3	424.8	536.6	14 03 25.77	54 22 36.7	72.33 ± 3.28	25.53 ± 0.06	24.48 ± 0.09
103.....	3	520.8	547.1	14 03 25.21	54 22 45.1	2.45 ± 0.00	22.94 ± 0.01	21.75 ± 0.03
104.....	3	500.5	550.1	14 03 25.38	54 22 43.6	7.47 ± 0.01	25.06 ± 0.03	22.25 ± 0.02
105.....	3	684.9	558.7	14 03 24.19	54 22 59.1	2.74 ± 0.00	25.37 ± 0.05	24.14 ± 0.05
106.....	3	557.5	561.7	14 03 25.10	54 22 48.9	14.35 ± 0.01	24.55 ± 0.04	23.55 ± 0.05
107.....	3	669.5	566.2	14 03 24.37	54 22 58.3	15.54 ± 0.05	24.93 ± 0.02	23.92 ± 0.05
108.....	3	218.8	572.2	14 03 27.52	54 22 22.1	2.29 ± 0.00	24.83 ± 0.03	23.83 ± 0.06
109.....	3	241.9	577.2	14 03 27.41	54 22 24.2	62.69 ± 1.03	26.38 ± 0.05	24.23 ± 0.04
110.....	3	270.0	578.2	14 03 27.23	54 22 26.6	2.92 ± 0.00	26.40 ± 0.08	25.66 ± 0.13
111.....	3	640.9	580.7	14 03 24.70	54 22 56.9	35.37 ± 0.03	23.50 ± 0.01	22.48 ± 0.02
112.....	3	453.8	592.8	14 03 26.10	54 22 42.4	81.16 ± 9.85	23.89 ± 0.09	21.98 ± 0.10
113.....	3	362.2	595.1	14 03 26.75	54 22 35.1	4.18 ± 0.01	25.33 ± 0.05	22.89 ± 0.04
114.....	3	312.0	611.8	14 03 27.25	54 22 32.0	9.56 ± 0.04	25.51 ± 0.04	24.50 ± 0.06
115.....	3	603.8	618.0	14 03 25.30	54 22 56.1	18.25 ± 0.02	24.59 ± 0.02	22.79 ± 0.03
116.....	3	764.1	619.7	14 03 24.21	54 23 09.2	7.74 ± 0.02	25.55 ± 0.03	22.38 ± 0.02
117.....	3	213.8	625.9	14 03 28.06	54 22 24.9	9.44 ± 0.01	25.03 ± 0.02	23.89 ± 0.05
118.....	3	314.8	633.0	14 03 27.43	54 22 33.5	5.22 ± 0.00	25.23 ± 0.05	24.38 ± 0.10
119.....	3	262.2	637.3	14 03 27.83	54 22 29.5	71.03 ± 0.93	23.85 ± 0.01	23.15 ± 0.03
120.....	3	377.5	638.3	14 03 27.05	54 22 38.9	47.03 ± 0.17	23.80 ± 0.02	22.77 ± 0.03
121.....	3	732.9	652.3	14 03 24.73	54 23 08.6	45.94 ± 0.15	23.75 ± 0.01	22.61 ± 0.03
122.....	3	365.8	654.3	14 03 27.27	54 22 38.9	22.30 ± 0.02	24.81 ± 0.03	23.64 ± 0.05
123.....	3	328.8	660.0	14 03 27.58	54 22 36.3	7.72 ± 0.02	24.52 ± 0.02	22.69 ± 0.02
124.....	3	95.9	674.8	14 03 29.32	54 22 18.3	4.07 ± 0.01	24.39 ± 0.04	22.83 ± 0.05
125.....	3	203.8	711.7	14 03 28.92	54 22 29.2	4.13 ± 0.05	23.82 ± 0.03	21.05 ± 0.03
126.....	3	475.5	741.6	14 03 27.33	54 22 53.1	20.00 ± 0.02	24.58 ± 0.02	23.50 ± 0.03
127.....	3	389.4	746.4	14 03 27.97	54 22 46.4	7.40 ± 0.05	25.08 ± 0.04	22.15 ± 0.03
128.....	3	730.1	751.7	14 03 25.67	54 23 14.4	30.30 ± 0.03	24.06 ± 0.02	22.98 ± 0.04
129.....	3	199.9	773.2	14 03 29.52	54 22 32.6	51.80 ± 0.14	23.62 ± 0.01	22.28 ± 0.02
130.....	3	569.1	783.0	14 03 27.07	54 23 03.2	3.42 ± 0.00	25.55 ± 0.03	24.30 ± 0.09
131.....	3	744.6	792.3	14 03 25.95	54 23 18.0	16.94 ± 0.02	23.93 ± 0.02	23.34 ± 0.04
132.....	3	249.0	795.0	14 03 29.39	54 22 37.9	13.44 ± 0.15	26.48 ± 0.11	24.52 ± 0.10
133.....	3	144.7	802.9	14 03 30.18	54 22 29.9	11.84 ± 0.02	24.60 ± 0.03	21.91 ± 0.03
134.....	3	58.0	821.1	14 03 30.94	54 22 24.0	100.9 ± 0.78	25.16 ± 0.03	24.55 ± 0.10
135.....	4	444.1	101.1	14 03 28.04	54 21 54.7	13.93 ± 0.04	25.85 ± 0.05	24.34 ± 0.06
136.....	4	499.2	102.0	14 03 28.56	54 21 57.9	16.58 ± 0.03	24.50 ± 0.03	24.15 ± 0.07
137.....	4	790.7	103.1	14 03 31.28	54 22 15.3	23.83 ± 0.03	24.47 ± 0.02	22.95 ± 0.03
138.....	4	244.1	106.8	14 03 26.22	54 21 42.2	5.09 ± 0.00	25.09 ± 0.03	24.65 ± 0.08
139.....	4	146.2	108.3	14 03 25.32	54 21 36.2	4.93 ± 0.01	25.98 ± 0.05	24.32 ± 0.07
140.....	4	505.0	108.3	14 03 28.66	54 21 57.7	20.82 ± 0.05	23.78 ± 0.02	22.28 ± 0.02
141.....	4	263.9	117.9	14 03 26.48	54 21 42.5	12.74 ± 0.01	24.81 ± 0.03	23.66 ± 0.04
142.....	4	714.9	126.0	14 03 30.73	54 22 08.9	15.64 ± 0.06	26.94 ± 0.13	23.92 ± 0.27
143.....	4	637.8	126.5	14 03 30.02	54 22 04.2	5.57 ± 0.01	25.00 ± 0.03	22.07 ± 0.03
144.....	4	563.6	126.7	14 03 29.33	54 21 59.8	22.21 ± 0.07	25.33 ± 0.05	23.80 ± 0.08
145.....	4	451.8	127.5	14 03 28.30	54 21 53.0	18.15 ± 0.02	24.33 ± 0.02	23.51 ± 0.05

TABLE 3—*Continued*

ID	Chip	X (pixels)	Y (pixels)	R.A. (J2000)	decl. (J2000)	P (days)	$\langle V \rangle$ (mag)	$\langle I \rangle$ (mag)
146.....	4	700.5	136.1	14 03 30.67	54 22 07.2	71.50 ± 0.47	22.83 ± 0.02	21.84 ± 0.02
147.....	4	595.8	137.0	14 03 29.70	54 22 00.9	3.83 ± 0.00	25.82 ± 0.04	24.09 ± 0.04
148.....	4	158.5	139.3	14 03 25.65	54 21 34.4	2.35 ± 0.02	26.38 ± 0.08	23.86 ± 0.04
149.....	4	730.2	147.2	14 03 31.02	54 22 08.1	11.09 ± 0.01	24.86 ± 0.02	23.77 ± 0.02
150.....	4	386.1	150.3	14 03 27.84	54 21 47.2	7.64 ± 0.06	24.07 ± 0.02	21.56 ± 0.02
151.....	4	343.2	158.9	14 03 27.50	54 21 43.9	7.82 ± 0.02	26.16 ± 0.07	22.65 ± 0.02
152.....	4	608.9	163.1	14 03 30.00	54 21 59.5	104.3 ± 1.50	24.25 ± 0.02	21.65 ± 0.02
153.....	4	628.9	183.9	14 03 30.33	54 21 59.0	18.20 ± 0.01	24.84 ± 0.02	23.80 ± 0.05
154.....	4	558.7	193.0	14 03 29.74	54 21 54.1	102.6 ± 17.6	23.22 ± 0.02	20.43 ± 0.02
155.....	4	475.8	200.9	14 03 29.02	54 21 48.5	15.27 ± 0.03	24.54 ± 0.02	23.63 ± 0.04
156.....	4	400.9	204.6	14 03 28.35	54 21 43.7	3.11 ± 0.00	25.88 ± 0.04	25.02 ± 0.09
157.....	4	382.7	207.2	14 03 28.20	54 21 42.4	17.33 ± 0.03	25.49 ± 0.04	24.47 ± 0.10
158.....	4	181.7	209.1	14 03 26.35	54 21 30.1	102.8 ± 0.77	25.44 ± 0.03	21.95 ± 0.02
159.....	4	754.4	210.1	14 03 31.67	54 22 04.5	2.50 ± 0.00	25.63 ± 0.04	24.97 ± 0.08
160.....	4	813.9	211.8	14 03 32.24	54 22 07.9	32.21 ± 0.19	23.50 ± 0.01	22.73 ± 0.03
161.....	4	309.4	213.9	14 03 27.57	54 21 37.4	23.85 ± 0.10	24.36 ± 0.02	23.33 ± 0.03
162.....	4	314.4	219.6	14 03 27.65	54 21 37.3	12.63 ± 0.02	25.02 ± 0.03	23.94 ± 0.05
163.....	4	282.5	221.6	14 03 27.37	54 21 35.2	9.13 ± 0.01	24.66 ± 0.08	24.10 ± 0.14
164.....	4	581.9	221.9	14 03 30.15	54 21 53.1	11.80 ± 0.01	25.24 ± 0.02	24.17 ± 0.04
165.....	4	625.9	228.9	14 03 30.61	54 21 55.2	11.17 ± 0.01	24.78 ± 0.02	23.97 ± 0.03
166.....	4	720.0	235.2	14 03 31.53	54 22 00.4	6.29 ± 0.00	25.73 ± 0.04	24.69 ± 0.09
167.....	4	422.3	240.3	14 03 28.80	54 21 42.1	5.49 ± 0.00	22.27 ± 0.01	21.66 ± 0.01
168.....	4	576.5	243.4	14 03 30.25	54 21 51.1	14.20 ± 0.05	24.93 ± 0.02	23.44 ± 0.03
169.....	4	724.6	247.6	14 03 31.66	54 21 59.6	9.65 ± 0.01	25.08 ± 0.02	23.94 ± 0.03
170.....	4	478.5	249.4	14 03 29.38	54 21 44.7	17.60 ± 0.06	25.32 ± 0.03	23.76 ± 0.04
171.....	4	444.7	261.5	14 03 29.15	54 21 41.7	7.65 ± 0.01	24.31 ± 0.05	23.79 ± 0.09
172.....	4	538.7	263.5	14 03 30.04	54 21 47.2	15.44 ± 0.06	24.92 ± 0.02	23.84 ± 0.04
173.....	4	695.5	263.9	14 03 31.50	54 21 56.5	2.56 ± 0.00	25.30 ± 0.03	24.38 ± 0.04
174.....	4	177.1	267.6	14 03 26.71	54 21 25.1	15.29 ± 0.03	24.75 ± 0.03	23.85 ± 0.05
175.....	4	538.2	269.1	14 03 30.07	54 21 46.7	7.98 ± 0.01	25.73 ± 0.05	24.92 ± 0.08
176.....	4	285.8	294.3	14 03 27.90	54 21 29.5	8.28 ± 0.02	24.75 ± 0.04	24.84 ± 0.14
177.....	4	370.0	302.0	14 03 28.73	54 21 33.9	2.27 ± 0.00	25.57 ± 0.06	21.77 ± 0.04
178.....	4	556.5	304.3	14 03 30.48	54 21 44.9	96.12 ± 0.56	22.47 ± 0.01	22.24 ± 0.02
179.....	4	253.6	307.0	14 03 27.69	54 21 26.5	105.6 ± 1.02	21.01 ± 0.01	20.28 ± 0.01
180.....	4	619.9	308.7	14 03 31.10	54 21 48.4	4.09 ± 0.00	25.65 ± 0.04	23.06 ± 0.04
181.....	4	327.3	309.8	14 03 28.39	54 21 30.7	2.19 ± 0.00	23.70 ± 0.04	21.46 ± 0.04
182.....	4	395.1	311.2	14 03 29.03	54 21 34.7	65.12 ± 0.73	23.00 ± 0.02	21.79 ± 0.03
183.....	4	337.7	321.3	14 03 28.57	54 21 30.4	21.15 ± 0.05	22.91 ± 0.01	22.78 ± 0.02
184.....	4	447.2	335.9	14 03 29.68	54 21 35.8	17.00 ± 0.13	24.42 ± 0.04	23.66 ± 0.04
185.....	4	203.9	340.4	14 03 27.45	54 21 20.8	54.31 ± 0.26	24.33 ± 0.03	23.34 ± 0.05
186.....	4	238.2	341.8	14 03 27.78	54 21 22.8	27.81 ± 0.08	25.14 ± 0.03	23.55 ± 0.04
187.....	4	655.3	344.4	14 03 31.68	54 21 47.6	13.66 ± 0.04	26.55 ± 0.07	22.84 ± 0.19
188.....	4	760.5	346.5	14 03 32.67	54 21 53.7	105.4 ± 0.95	24.59 ± 0.03	21.47 ± 0.02
189.....	4	444.5	348.4	14 03 29.74	54 21 34.6	37.71 ± 0.10	23.64 ± 0.03	22.67 ± 0.05
190.....	4	803.4	350.2	14 03 33.09	54 21 56.0	15.68 ± 0.04	24.87 ± 0.03	23.97 ± 0.05
191.....	4	448.3	350.6	14 03 29.80	54 21 34.7	13.08 ± 0.02	24.67 ± 0.02	23.95 ± 0.06
192.....	4	216.3	356.5	14 03 27.68	54 21 20.3	73.78 ± 0.38	23.00 ± 0.02	21.89 ± 0.02
193.....	4	211.6	364.6	14 03 27.69	54 21 19.3	77.74 ± 0.58	23.39 ± 0.07	23.49 ± 0.13
194.....	4	309.6	369.5	14 03 28.64	54 21 24.8	44.76 ± 0.18	24.26 ± 0.02	22.93 ± 0.03
195.....	4	574.8	371.3	14 03 31.11	54 21 40.6	13.35 ± 0.02	24.58 ± 0.02	23.84 ± 0.03
196.....	4	207.4	371.7	14 03 27.70	54 21 18.5	2.09 ± 0.00	23.61 ± 0.03	23.40 ± 0.05
197.....	4	175.4	374.8	14 03 27.43	54 21 16.3	93.32 ± 1.19	24.85 ± 0.04	21.99 ± 0.03
198.....	4	465.3	377.8	14 03 30.14	54 21 33.5	18.25 ± 0.05	24.51 ± 0.02	23.68 ± 0.04
199.....	4	467.7	381.6	14 03 30.19	54 21 33.3	2.24 ± 0.00	23.65 ± 0.04	23.33 ± 0.11
200.....	4	152.5	382.9	14 03 27.27	54 21 14.3	28.15 ± 0.09	24.10 ± 0.02	22.60 ± 0.04
201.....	4	473.6	386.8	14 03 30.28	54 21 33.2	22.26 ± 0.04	24.05 ± 0.03	23.36 ± 0.05
202.....	4	355.0	390.4	14 03 29.20	54 21 25.8	13.21 ± 0.01	24.25 ± 0.02	23.12 ± 0.07
203.....	4	359.0	391.9	14 03 29.25	54 21 25.9	4.28 ± 0.01	24.87 ± 0.04	23.98 ± 0.45
204.....	4	631.7	392.2	14 03 31.79	54 21 42.3	7.84 ± 0.00	25.28 ± 0.03	24.16 ± 0.06
205.....	4	208.4	398.6	14 03 27.90	54 21 16.4	26.06 ± 0.04	23.56 ± 0.01	22.80 ± 0.03
206.....	4	642.0	401.2	14 03 31.94	54 21 42.2	4.60 ± 0.09	24.29 ± 0.02	21.54 ± 0.03
207.....	4	314.2	403.2	14 03 28.91	54 21 22.3	31.91 ± 0.08	24.10 ± 0.02	23.16 ± 0.04
208.....	4	602.8	404.4	14 03 31.60	54 21 39.6	3.61 ± 0.00	25.04 ± 0.02	25.70 ± 0.13
209.....	4	211.7	408.9	14 03 28.00	54 21 15.7	94.01 ± 0.99	24.38 ± 0.09	23.69 ± 0.17
210.....	4	366.9	412.5	14 03 29.46	54 21 24.8	19.81 ± 0.04	24.37 ± 0.01	23.36 ± 0.03
211.....	4	538.8	415.1	14 03 31.08	54 21 34.9	38.15 ± 0.18	25.09 ± 0.04	23.97 ± 0.05
212.....	4	217.4	429.8	14 03 28.19	54 21 14.4	29.39 ± 0.10	24.09 ± 0.01	23.04 ± 0.01
213.....	4	691.3	430.8	14 03 32.60	54 21 42.7	17.02 ± 0.05	24.96 ± 0.02	24.17 ± 0.05
214.....	4	363.6	431.3	14 03 29.56	54 21 23.0	26.53 ± 0.09	25.52 ± 0.04	23.73 ± 0.04
215.....	4	797.6	434.0	14 03 33.61	54 21 48.9	12.99 ± 0.02	24.87 ± 0.01	23.96 ± 0.03
216.....	4	532.0	446.1	14 03 31.23	54 21 31.9	95.85 ± 0.35	24.01 ± 0.02	22.59 ± 0.03
217.....	4	189.1	451.6	14 03 28.08	54 21 10.9	14.87 ± 0.04	24.90 ± 0.03	24.07 ± 0.08
218.....	4	386.5	466.8	14 03 30.02	54 21 21.5	114.3 ± 2.63	25.46 ± 0.05	24.33 ± 0.06

TABLE 3—*Continued*

ID	Chip	X (pixels)	Y (pixels)	R.A. (J2000)	decl. (J2000)	P (days)	$\langle V \rangle$ (mag)	$\langle I \rangle$ (mag)
219.....	4	371.7	467.0	14 03 29.88	54 21 20.6	12.59 ± 0.02	24.58 ± 0.02	23.78 ± 0.04
220.....	4	411.8	483.8	14 03 30.37	54 21 21.7	22.38 ± 0.04	23.71 ± 0.01	22.89 ± 0.02
221.....	4	230.9	485.0	14 03 28.70	54 21 10.7	9.48 ± 0.01	24.36 ± 0.02	21.92 ± 0.02
222.....	4	602.2	501.5	14 03 32.26	54 21 31.7	22.97 ± 0.06	24.32 ± 0.03	23.35 ± 0.05
223.....	4	717.0	505.1	14 03 33.35	54 21 38.2	95.72 ± 0.90	24.81 ± 0.03	23.68 ± 0.04
224.....	4	222.9	505.3	14 03 28.76	54 21 08.6	11.47 ± 0.02	24.84 ± 0.02	23.95 ± 0.04
225.....	4	240.5	508.3	14 03 28.95	54 21 09.4	108.7 ± 16.9	24.01 ± 0.03	21.12 ± 0.04
226.....	4	342.5	518.5	14 03 29.97	54 21 14.7	25.79 ± 0.04	24.42 ± 0.02	23.41 ± 0.02
227.....	4	683.7	520.0	14 03 33.15	54 21 35.0	14.06 ± 0.02	25.80 ± 0.05	24.90 ± 0.10
228.....	4	771.9	520.5	14 03 33.97	54 21 40.3	2.18 ± 0.00	24.41 ± 0.05	22.87 ± 0.06
229.....	4	204.4	522.1	14 03 28.71	54 21 06.1	7.78 ± 0.02	26.00 ± 0.08	24.00 ± 0.06
230.....	4	340.9	533.0	14 03 30.05	54 21 13.4	21.09 ± 0.04	25.41 ± 0.04	24.12 ± 0.05
231.....	4	267.1	538.0	14 03 29.40	54 21 08.6	2.29 ± 0.00	22.33 ± 0.02	20.75 ± 0.02
232.....	4	242.8	545.4	14 03 29.23	54 21 06.5	7.53 ± 0.01	25.28 ± 0.04	24.42 ± 0.07
233.....	4	209.0	561.7	14 03 29.02	54 21 03.1	38.38 ± 0.06	23.65 ± 0.02	22.47 ± 0.03
234.....	4	811.5	568.4	14 03 34.67	54 21 38.8	12.24 ± 0.02	25.17 ± 0.02	24.03 ± 0.05
235.....	4	425.8	576.2	14 03 31.14	54 21 15.0	7.76 ± 0.01	24.75 ± 0.03	22.25 ± 0.02
236.....	4	800.7	598.3	14 03 34.77	54 21 35.7	2.36 ± 0.00	26.15 ± 0.11	23.56 ± 0.20
237.....	4	245.2	599.5	14 03 29.62	54 21 02.3	2.92 ± 0.00	25.07 ± 0.03	24.16 ± 0.04
238.....	4	444.8	613.6	14 03 31.57	54 21 13.1	2.16 ± 0.00	23.61 ± 0.05	23.68 ± 0.09
239.....	4	521.8	620.8	14 03 32.34	54 21 17.1	2.03 ± 0.00	26.40 ± 0.08	24.95 ± 0.10
240.....	4	461.9	625.6	14 03 31.81	54 21 13.1	3.34 ± 0.00	18.13 ± 0.02	18.39 ± 0.03
241.....	4	558.9	630.3	14 03 32.74	54 21 18.6	21.19 ± 0.03	23.95 ± 0.02	23.12 ± 0.03
242.....	4	468.1	631.5	14 03 31.91	54 21 13.0	2.22 ± 0.00	21.87 ± 0.05	21.45 ± 0.06
243.....	4	757.2	653.3	14 03 34.75	54 21 28.6	2.22 ± 0.00	24.36 ± 0.05	23.55 ± 0.07
244.....	4	349.7	669.2	14 03 31.07	54 21 02.9	35.99 ± 0.07	24.15 ± 0.02	22.94 ± 0.03
245.....	4	161.7	680.6	14 03 29.40	54 20 50.7	17.02 ± 0.02	23.16 ± 0.03	23.20 ± 0.05
246.....	4	291.1	686.6	14 03 30.64	54 20 57.9	92.71 ± 0.36	22.79 ± 0.01	21.69 ± 0.01
247.....	4	352.6	698.3	14 03 31.30	54 21 00.7	50.00 ± 0.31	23.96 ± 0.02	22.76 ± 0.03
248.....	4	121.1	717.4	14 03 29.28	54 20 45.2	54.26 ± 0.12	22.83 ± 0.01	21.76 ± 0.02
249.....	4	247.7	719.9	14 03 30.47	54 20 52.6	4.83 ± 0.01	25.60 ± 0.05	25.27 ± 0.12
250.....	4	381.5	730.4	14 03 31.78	54 20 59.8	55.34 ± 0.12	23.53 ± 0.01	22.38 ± 0.02
251.....	4	138.4	754.5	14 03 29.69	54 20 43.3	21.50 ± 0.02	23.72 ± 0.02	23.03 ± 0.04
252.....	4	568.9	769.0	14 03 33.79	54 21 07.9	11.55 ± 0.12	25.67 ± 0.05	23.97 ± 0.04
253.....	4	421.1	773.3	14 03 32.45	54 20 58.7	15.74 ± 0.01	24.88 ± 0.03	23.74 ± 0.06
254.....	4	750.4	800.5	14 03 35.69	54 21 16.3	67.13 ± 0.80	24.47 ± 0.09	21.86 ± 0.09
255.....	4	451.4	800.6	14 03 32.92	54 20 58.3	95.17 ± 0.52	23.78 ± 0.03	21.70 ± 0.02

NOTE.—Units of right ascension are hours, minutes, and seconds, and units of declination are degrees, arcminutes, and arcseconds.

and the differences in the mean V- and I-band magnitudes are $+0.001 \pm 0.008$ and $+0.004 \pm 0.009$ in the sense (DoPHOT − DAOPHOT); standard errors of the mean difference are quoted. Among these 93 stars, the lowest value of the WS93 variability index was 0.641, and the sample of ALLFRAME candidates was trimmed down from 279 to 255 stars using this value as a lower limit.

5. THE CEPHEID PL RELATIONS AND THE DISTANCE MODULUS

The V- and I-band PL relations derived from the DAOPHOT/ALLFRAME analysis are shown in Figure 3. Again, at this point we have chosen to apply *no* subjective selection—with possible hidden bias—on the sample, but plot all 255 candidates. Dashed curves in Figure 3 delineate the region of the PL diagram that will be considered in estimating the distance modulus of M101. Nine "perfect" Cepheids (all examiners gave each of them a score of 1 in both image quality and light-curve quality: variables 2, 6, 8, 11, 13, 19, 89, 139, and 234) are represented by five-pointed stars, while 99 other Cepheid candidates that lie within the dashed boundaries in *both* panels are denoted by filled circles: these 108 stars are the ones from which the PL relation will be estimated. Candidate variables lying outside the dashed boundaries in at least one panel are shown as triangles (105 stars with periods less than 20 days) or squares (42 stars with periods longer than 20 days). Symbol size is coded to our subjective combined quality index, decreasing as the score increases from 1.1 to 4.0.

Within a certain range of periods, a rather diffuse V-band PL relation is perceived, as is a somewhat sharper I-band relation. A number of short-period and long-period variables—some with quite high subjective quality scores—are also seen; some of these lie near the extrapolation of the mean PL relations, but others lie completely off them. Little of the scatter in the perceived PL relations is due to observational errors. More is due to the finite width of the instability strip, but much or most of it, as a quick glance at an image of the center of M101 will show, must be due to differential reddening within the galaxy. Stars above the sloping dashed lines are too luminous to be normal classical Cepheids. There seem to be more stars that are anomalously bright in the I-band than in V, but this may simply be due to the fact that, with only four long exposures and one short exposure, the mean I-band magnitudes are more vulnerable than those in V to corruption by cosmic rays or other blunders.

The upper panel of Figure 4 is the color magnitude for 16,612 stars in the inner field of M101 with photometric standard errors $\sigma(V-I) \leq 0.30$ mag. The lower panel is the equivalent color-magnitude diagram for the 255 variable candidates. As hoped, the good Cepheid candidates popu-

TABLE 4

SUBJECTIVE QUALITY SCORES FOR VARIABLE CANDIDATES

ID	Image Quality	Light-Curve Quality	Combined Quality
1	1.00	1.40	1.20
2	1.00	1.00	1.00
3	1.75	1.40	1.58
4	1.25	1.20	1.23
5	1.75	1.00	1.38
6	1.00	1.00	1.00
7	1.75	1.40	1.58
8	1.00	1.00	1.00
9	1.25	3.00	2.12
10.....	1.00	1.40	1.20
11.....	1.00	1.00	1.00
12.....	1.00	1.00	1.00
13.....	2.50	2.80	2.65
14.....	2.25	3.00	2.62
15.....	1.25	1.60	1.42
16.....	1.00	2.80	1.90
17.....	1.75	2.80	2.28
18.....	1.00	1.00	1.00
19.....	3.25	2.20	2.72
20.....	3.00	2.40	2.70
21.....	2.75	1.00	1.88
22.....	2.75	2.60	2.67
23.....	2.50	1.20	1.85
24.....	4.00	3.20	3.60
25.....	3.25	1.40	2.33
26.....	2.25	1.60	1.92
27.....	4.00	2.80	3.40
28.....	2.75	2.80	2.78
29.....	2.50	2.80	2.65
30.....	2.50	1.00	1.75
31.....	3.50	2.60	3.05
32.....	4.00	3.60	3.80
33.....	2.50	1.00	1.75
34.....	1.50	3.20	2.35
35.....	2.00	2.60	2.30
36.....	1.25	1.00	1.12
37.....	3.00	3.20	3.10
38.....	2.00	2.40	2.20
39.....	2.75	3.00	2.88
40.....	3.75	3.00	3.38
41.....	1.50	1.00	1.25
42.....	1.25	1.40	1.33
43.....	2.75	2.20	2.47
44.....	3.75	3.80	3.78
45.....	1.50	1.60	1.55
46.....	2.50	1.60	2.05
47.....	3.00	3.40	3.20
48.....	2.50	3.40	2.95
49.....	2.50	2.80	2.65
50.....	2.00	1.20	1.60
51.....	3.00	1.00	2.00
52.....	1.75	1.60	1.67
53.....	2.50	2.20	2.35
54.....	2.25	3.80	3.03
55.....	3.75	3.20	3.47
56.....	1.75	2.80	2.28
57.....	2.75	3.40	3.08
58.....	3.75	4.00	3.88
59.....	2.00	2.20	2.10
60.....	2.50	1.60	2.05
61.....	3.50	3.80	3.65
62.....	3.00	1.60	2.30
63.....	2.25	1.80	2.03
64.....	2.00	1.80	1.90
65.....	2.00	3.80	2.90
66.....	2.00	2.20	2.10
67.....	2.50	2.80	2.65
68.....	2.50	1.20	1.85
69.....	1.75	2.00	1.88
70.....	2.50	1.80	2.15
71.....	3.75	3.80	3.78

TABLE 4—*Continued*

ID	Image Quality	Light-Curve Quality	Combined Quality
73	1.75	1.60	1.67
74	1.75	1.00	1.38
75	4.00	4.00	4.00
76	1.75	2.80	2.28
77	2.00	1.00	1.50
78	1.50	1.00	1.25
79	3.00	3.20	3.10
80	3.00	3.20	3.10
81	1.00	1.00	1.00
82	3.75	3.40	3.58
83	1.75	2.60	2.17
84	2.75	1.00	1.88
85	3.25	3.40	3.33
86	3.50	3.60	3.55
87	1.00	3.20	2.10
88	1.25	1.20	1.23
89	2.75	3.40	3.08
90	2.50	3.60	3.05
91	2.75	1.80	2.28
92	2.75	3.80	3.28
93	2.00	1.00	1.50
94	2.75	1.40	2.08
95	2.00	1.00	1.50
96	3.50	3.00	3.25
97	3.00	1.00	2.00
98	3.25	3.80	3.53
99	2.25	3.20	2.72
100.....	1.00	1.60	1.30
101.....	1.25	1.00	1.12
102.....	3.00	2.20	2.60
103.....	2.75	3.40	3.08
104.....	1.75	2.80	2.28
105.....	1.50	3.20	2.35
106.....	2.25	1.00	1.62
107.....	2.75	1.00	1.88
108.....	1.00	3.00	2.00
109.....	3.75	2.60	3.17
110.....	3.75	3.60	3.67
111.....	1.75	1.00	1.38
112.....	4.00	4.00	4.00
113.....	3.00	3.60	3.30
114.....	1.75	1.80	1.77
115.....	1.25	2.00	1.62
116.....	1.75	2.60	2.17
117.....	1.25	2.20	1.73
118.....	1.75	3.60	2.67
119.....	1.00	1.80	1.40
120.....	2.75	1.20	1.98
121.....	2.25	1.00	1.62
122.....	1.25	1.20	1.23
123.....	1.50	2.60	2.05
124.....	1.75	3.60	2.67
125.....	2.25	3.80	3.03
126.....	1.00	1.00	1.00
127.....	2.25	3.80	3.03
128.....	2.50	1.00	1.75
129.....	1.25	1.20	1.23
130.....	1.75	2.00	1.88
131.....	3.00	1.00	2.00
132.....	3.75	3.40	3.58
133.....	2.50	2.40	2.45
134.....	1.50	3.00	2.25
135.....	3.00	3.20	3.10
136.....	2.50	3.00	2.75
137.....	1.25	1.20	1.23
138.....	1.75	1.80	1.77
139.....	3.25	3.20	3.22
140.....	3.00	1.00	2.00
141.....	2.75	1.60	2.17
142.....	3.50	3.40	3.45
143.....	2.25	3.00	2.62
144.....	3.50	1.80	2.65
145.....	1.75	1.00	1.38

TABLE 4—*Continued*

ID	Image Quality	Light-Curve Quality	Combined Quality
146.....	1.75	1.80	1.77
147.....	3.50	3.20	3.35
148.....	4.00	3.80	3.90
149.....	1.75	1.20	1.48
150.....	2.00	3.80	2.90
151.....	3.50	3.60	3.55
152.....	2.00	2.60	2.30
153.....	1.75	1.40	1.58
154.....	1.00	3.20	2.10
155.....	2.25	1.40	1.83
156.....	4.00	3.20	3.60
157.....	3.50	2.80	3.15
158.....	2.00	2.40	2.20
159.....	3.00	3.60	3.30
160.....	3.00	1.00	2.00
161.....	1.25	1.00	1.12
162.....	1.75	1.40	1.58
163.....	4.00	3.40	3.70
164.....	2.50	1.40	1.95
165.....	1.75	2.00	1.88
166.....	2.50	2.00	2.25
167.....	1.75	2.20	1.98
168.....	1.75	1.00	1.38
169.....	1.75	1.60	1.67
170.....	1.50	1.20	1.35
171.....	2.50	3.00	2.75
172.....	2.00	1.40	1.70
173.....	2.50	2.00	2.25
174.....	2.50	1.00	1.75
175.....	3.00	2.60	2.80
176.....	2.50	3.20	2.85
177.....	3.75	3.40	3.58
178.....	1.50	3.40	2.45
179.....	1.75	2.80	2.28
180.....	2.00	2.80	2.40
181.....	3.25	3.40	3.33
182.....	2.75	1.60	2.17
183.....	3.00	2.00	2.50
184.....	2.25	2.20	2.22
185.....	2.75	1.40	2.08
186.....	3.25	1.60	2.42
187.....	2.75	3.20	2.97
188.....	2.50	2.20	2.35
189.....	1.75	1.40	1.58
190.....	1.75	1.20	1.48
191.....	2.50	1.60	2.05
192.....	1.75	2.40	2.08
193.....	3.25	3.40	3.33
194.....	2.50	2.60	2.55
195.....	2.00	1.00	1.50
196.....	3.00	3.20	3.10
197.....	1.75	3.00	2.38
198.....	1.75	1.20	1.48
199.....	1.75	2.60	2.17
200.....	2.50	1.20	1.85
201.....	2.00	1.00	1.50
202.....	2.25	1.00	1.62
203.....	2.50	2.60	2.55
204.....	2.50	1.40	1.95
205.....	2.50	1.00	1.75
206.....	1.75	3.80	2.78
207.....	2.50	1.00	1.75
208.....	1.50	3.20	2.35
209.....	4.00	3.20	3.60
210.....	1.50	1.20	1.35
211.....	1.50	1.40	1.45
212.....	2.50	1.20	1.85
213.....	1.00	1.40	1.20
214.....	2.75	1.80	2.28
215.....	1.00	1.00	1.00
216.....	1.25	2.60	1.92
217.....	1.25	1.40	1.33
218.....	2.25	2.60	2.42

TABLE 4—*Continued*

ID	Image Quality	Light-Curve Quality	Combined Quality
219.....	2.00	1.80	1.90
220.....	2.00	1.00	1.50
221.....	2.50	2.00	2.25
222.....	2.25	1.20	1.73
223.....	1.25	2.00	1.62
224.....	2.75	1.60	2.17
225.....	2.75	3.60	3.17
226.....	2.50	1.40	1.95
227.....	2.50	2.80	2.65
228.....	1.75	3.00	2.38
229.....	2.25	3.20	2.72
230.....	1.25	1.60	1.42
231.....	2.50	3.00	2.75
232.....	2.00	2.00	2.00
233.....	1.00	1.40	1.20
234.....	3.00	1.40	2.20
235.....	2.25	3.80	3.03
236.....	3.50	3.80	3.65
237.....	1.75	3.20	2.47
238.....	4.00	3.20	3.60
239.....	2.75	3.60	3.17
240.....	4.00	3.60	3.80
241.....	1.00	1.60	1.30
242.....	4.00	3.20	3.60
243.....	2.00	3.60	2.80
244.....	1.50	1.00	1.25
245.....	2.50	2.60	2.55
246.....	2.75	1.80	2.28
247.....	1.25	1.20	1.23
248.....	2.75	1.20	1.98
249.....	3.00	3.80	3.40
250.....	1.25	1.00	1.12
251.....	2.25	1.00	1.62
252.....	2.25	2.60	2.42
253.....	2.50	1.40	1.95
254.....	2.25	3.40	2.83
255.....	1.75	2.20	1.98
72	2.50	3.20	2.85

late the Hertzsprung gap in the center of the diagram, while some of the long-period candidates (*open squares*) lie near the bright red end of the Cepheid population and some of the short-period variables (*open triangles*) lie faintward and toward the blue. In and above the blue plume in the color-magnitude diagram are a number of short-period and a few long-period variable candidates. The fainter ones may be young eclipsing binaries while the more luminous ones are, perhaps, Hubble-Sandage variables. Along the luminous fringe of the red supergiant population are a number of long-period and—astonishingly—short-period variable candidates. The former can easily be understood as Mira-type and other long-period evolved variable stars, but the short-period candidates are more puzzling. None of the candidate variables with $V-I > 2.0$ and $P < 20$ days has a combined image and light-curve quality as good as 2.0. The three best cases, candidates 9, 83, and 116, have scores between 2.1 and 2.2. In the case of candidate 9, it happens that all three of the faint V-band observations were obtained during the 1995 observing season, so it is most likely that the star faded by roughly 1 mag between 1994 and 1995. Candidates 83 and 116 show more convincing evidence of real short-term variation that is perceptible in both the V and I data. It is possible that these are real Cepheids or short-period variables of some other type that just happen to be blended with much redder stars, because their amplitudes are near the low extreme of that commonly

TABLE 5

COMPARISON OF ALLFRAME AND DoPHOT

	DoPHOT			DoPHOT-ALLFRAME		
ID	P (days)	$\langle V \rangle$ (mag)	$\langle I \rangle$ (mag)	$\Delta \log P$ (days)	$\Delta\langle V \rangle$ (mag)	$\Delta\langle I \rangle$ (mag)
2	42.0	23.43	22.51	0.00	-0.04 ± 0.03	0.05 ± 0.05
5	20.7	24.25	23.38	0.00	0.05 ± 0.08	-0.07 ± 0.08
7	16.0	24.81	24.02	0.03	-0.03 ± 0.08	0.14 ± 0.11
8	24.0	24.39	23.29	0.02	-0.05 ± 0.07	-0.14 ± 0.13
11	23.0	24.85	23.74	0.02	0.10 ± 0.08	0.15 ± 0.07
12	34.0	25.02	23.44	-0.01	0.08 ± 0.10	0.04 ± 0.08
16	12.8	25.17	24.11	0.00	0.05 ± 0.09	-0.05 ± 0.08
17	37.4	24.81	24.80	0.00	0.06 ± 0.07	0.12 ± 0.19
19	17.0	24.31	23.47	0.02	0.08 ± 0.06	0.08 ± 0.17
53	13.5	25.03	23.92	0.00	0.06 ± 0.11	-0.02 ± 0.14
56	14.0	24.92	24.22	-0.01	-0.04 ± 0.08	0.08 ± 0.13
57	11.5	25.47	24.36	-0.01	-0.16 ± 0.09	-0.03 ± 0.15
58	15.0	25.16	24.25	0.02	0.05 ± 0.13	0.00 ± 0.10
60	27.3	24.49	23.59	-0.02	-0.06 ± 0.06	0.08 ± 0.08
61	12.4	25.05	23.98	0.02	-0.11 ± 0.09	-0.56 ± 0.40
62	17.5	23.96	23.00	0.01	-0.04 ± 0.05	-0.05 ± 0.06
63	17.5	24.50	23.51	0.00	-0.07 ± 0.06	-0.03 ± 0.06
64	9.9	24.75	24.10	0.01	-0.09 ± 0.07	-0.16 ± 0.10
65	13.0	24.82	23.94	0.00	-0.06 ± 0.09	-0.02 ± 0.08
67	19.2	25.11	23.87	0.01	-0.07 ± 0.09	-0.07 ± 0.10
69	14.8	24.86	24.02	-0.01	-0.05 ± 0.07	-0.04 ± 0.22
71	31.0	23.60	22.74	-0.02	-0.03 ± 0.03	0.11 ± 0.04
72	35.0	23.82	22.80	0.00	-0.05 ± 0.08	-0.12 ± 0.21
78	11.0	24.81	24.25	0.01	-0.09 ± 0.06	0.13 ± 0.13
86	7.5	25.03	22.20	0.00	-0.04 ± 0.08	-0.05 ± 0.08
98	14.4	24.80	23.94	-0.02	0.04 ± 0.05	-0.03 ± 0.09
105.....	26.0	24.33	23.35	0.00	-0.03 ± 0.04	-0.03 ± 0.07
106.....	3.2	24.36	23.55	0.00	-0.07 ± 0.05	-0.04 ± 0.09
110.....	71.0	23.78	23.17	0.00	-0.07 ± 0.03	0.02 ± 0.04
111.....	16.0	25.61	24.06	0.02	0.11 ± 0.11	-0.02 ± 0.12
116.....	6.4	25.21	24.56	0.00	-0.02 ± 0.10	0.01 ± 0.20
118.....	15.6	24.96	24.03	0.00	0.03 ± 0.08	0.11 ± 0.12
120.....	45.0	23.80	22.59	-0.02	0.00 ± 0.05	-0.18 ± 0.07
121.....	14.0	24.55	23.82	0.01	-0.07 ± 0.06	-0.06 ± 0.09
122.....	22.3	24.71	23.74	0.00	-0.10 ± 0.06	0.10 ± 0.10
123.....	45.0	23.99	22.93	0.03	-0.14 ± 0.04	0.12 ± 0.08
124.....	14.4	24.46	23.45	0.00	-0.10 ± 0.08	-0.09 ± 0.08
125.....	20.4	24.46	23.71	-0.01	0.01 ± 0.06	0.04 ± 0.10
127.....	31.0	23.98	23.03	0.01	-0.08 ± 0.05	0.05 ± 0.08
128.....	16.8	24.60	24.02	0.01	0.01 ± 0.06	0.42 ± 0.20
129.....	50.0	23.72	22.69	0.04	-0.02 ± 0.03	0.08 ± 0.07
131.....	19.0	24.76	23.49	-0.02	0.18 ± 0.07	-0.02 ± 0.05
132.....	22.5	24.36	23.37	0.05	0.11 ± 0.06	-0.03 ± 0.11
133.....	18.0	24.24	23.35	0.00	-0.07 ± 0.06	-0.10 ± 0.11
134.....	35.0	23.46	22.37	0.00	-0.03 ± 0.03	-0.10 ± 0.05
135.....	17.3	25.75	24.56	0.00	0.26 ± 0.16	0.09 ± 0.19
141.....	60.0	23.06	21.86	-0.04	0.05 ± 0.04	0.06 ± 0.05
149.....	11.0	25.09	24.06	-0.02	0.25 ± 0.13	0.11 ± 0.12
150.....	21.1	25.56	24.25	0.00	0.15 ± 0.10	0.12 ± 0.12
151.....	12.2	25.24	24.03	0.00	0.07 ± 0.07	-0.01 ± 0.16
155.....	44.8	24.36	22.95	0.00	0.11 ± 0.05	0.02 ± 0.07
167.....	9.7	25.18	23.87	0.00	0.09 ± 0.08	-0.07 ± 0.06
171.....	14.2	24.94	23.39	0.00	0.01 ± 0.07	-0.05 ± 0.08
172.....	29.4	24.04	22.98	0.00	-0.05 ± 0.04	-0.06 ± 0.04
183.....	7.8	25.31	24.22	0.00	0.03 ± 0.09	0.06 ± 0.12
189.....	13.0	24.94	23.98	0.00	0.07 ± 0.06	0.02 ± 0.07
191.....	15.0	24.92	23.77	-0.01	0.00 ± 0.07	-0.07 ± 0.07
198.....	11.3	25.31	24.21	-0.02	0.07 ± 0.10	0.04 ± 0.11
201.....	12.9	24.84	23.77	0.01	0.02 ± 0.09	0.11 ± 0.07
202.....	27.0	24.17	22.68	-0.02	0.07 ± 0.07	0.08 ± 0.05
203.....	11.1	24.80	23.77	0.00	-0.06 ± 0.07	0.00 ± 0.05
204.....	31.5	25.09	23.59	0.05	-0.05 ± 0.08	0.04 ± 0.12
205.....	13.0	24.99	23.91	0.01	-0.02 ± 0.08	-0.03 ± 0.11
207.....	26.5	25.95	24.05	0.00	0.44 ± 0.17	0.32 ± 0.10
208.....	36.0	23.81	22.80	-0.02	0.17 ± 0.08	0.14 ± 0.09
209.....	54.3	22.93	21.87	0.00	0.09 ± 0.03	0.11 ± 0.06
210.....	15.7	24.87	24.00	0.00	0.00 ± 0.07	0.03 ± 0.09
213.....	16.1	24.91	24.10	-0.02	-0.04 ± 0.06	-0.06 ± 0.10
214.....	38.2	25.17	23.86	0.00	0.09 ± 0.10	-0.10 ± 0.22
217.....	24.7	23.82	22.80	-0.02	0.26 ± 0.05	0.00 ± 0.08

TABLE 5—*Continued*

	DoPHOT			DoPHOT-ALLFRAME		
ID	P (days)	$\langle V\rangle$ (mag)	$\langle I\rangle$ (mag)	$\Delta \log P$ (days)	$\Delta\langle V\rangle$ (mag)	$\Delta\langle I\rangle$ (mag)
220.....	18.5	25.34	23.76	0.02	0.02 ± 0.09	0.00 ± 0.09
222.....	22.2	25.36	23.87	0.00	0.04 ± 0.14	0.07 ± 0.22
225.....	19.0	23.97	23.21	−0.05	0.02 ± 0.04	0.09 ± 0.72
227.....	15.5	24.63	23.87	0.01	-0.12 ± 0.08	0.02 ± 0.10
228.....	19.3	24.40	23.38	−0.01	0.03 ± 0.04	0.01 ± 0.11
231.....	13.3	24.85	23.88	0.01	0.18 ± 0.08	-0.07 ± 0.08
232.....	18.2	24.86	23.54	0.00	0.02 ± 0.07	-0.27 ± 0.38
236.....	13.5	24.64	23.92	0.00	0.05 ± 0.06	0.08 ± 0.06
237.....	23.3	23.74	23.02	0.02	0.03 ± 0.04	0.13 ± 0.12
238.....	37.0	23.73	22.60	−0.02	0.08 ± 0.03	0.13 ± 0.10
239.....	22.0	24.00	23.31	−0.01	-0.05 ± 0.06	-0.05 ± 0.09
240.....	23.5	24.28	23.25	−0.01	-0.08 ± 0.05	-0.08 ± 0.05
241.....	23.0	24.43	22.98	−0.02	-0.03 ± 0.05	0.03 ± 0.06
242.....	11.0	24.79	24.00	−0.01	0.01 ± 0.05	0.03 ± 0.07
243.....	52.0	23.60	22.40	−0.03	0.07 ± 0.04	0.02 ± 0.12
245.....	23.0	24.29	22.92	0.00	-0.03 ± 0.05	-0.43 ± 0.18
246.....	15.0	24.91	23.88	0.00	0.01 ± 0.09	-0.19 ± 0.27
247.....	18.0	24.56	23.76	−0.01	0.05 ± 0.12	0.08 ± 0.15
249.....	32.2	23.45	22.59	0.00	-0.05 ± 0.04	-0.15 ± 0.05
250.....	35.0	24.24	22.94	−0.01	0.10 ± 0.06	0.00 ± 0.05
252.....	31.5	24.16	23.26	−0.01	0.06 ± 0.06	0.10 ± 0.06
253.....	18.0	24.22	23.37	0.00	-0.11 ± 0.05	-0.13 ± 0.07
254.....	19.5	23.72	22.16	−0.03	-0.06 ± 0.04	-0.12 ± 0.08

found in high-quality Cepheids (both have V-band semiamplitudes in the fundamental Fourier component of 0.26 mag; Stetson (1996) found that the effective lower limit for good-quality Cepheids in the Milky Way, the Magellanic Clouds, and the dwarf irregular galaxy IC 4182 was around 0.20 mag, while typical semiamplitudes were more like 0.4 mag). Therefore, some of the red variables possibly can be explained as legitimate Cepheids blended with red giants. Note, however, that only three of the candidate Cepheids (those within the dashed boundaries in *both* PL relations; *filled circles*) have $V-I > 1.8$, and those three have quite poor subjective quality scores. Many of the short-period variable candidates with red colors may simply reflect the

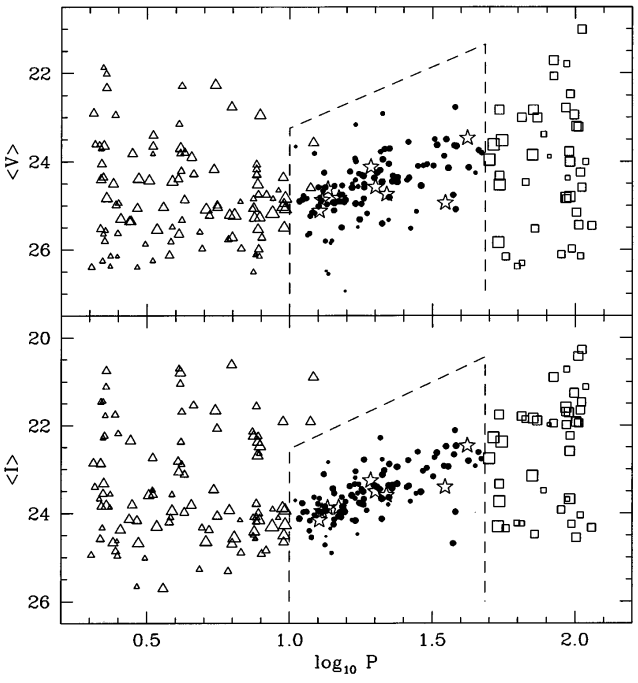

FIG. 3.—Apparent period-luminosity relations for 255 variable stars found in the inner field of M101. The upper panel shows the V-band PL relation, and the lower panel shows the I-band relation. Nine "perfect" Cepheid variables (*five-pointed stars*). An additional 99 Cepheid candidates within the period range 10–48.4 days (*filled circles*). 105 other candidate variables with periods less than 20 days (*triangles*). 42 other candidate variables with periods greater than 20 days (*squares*).

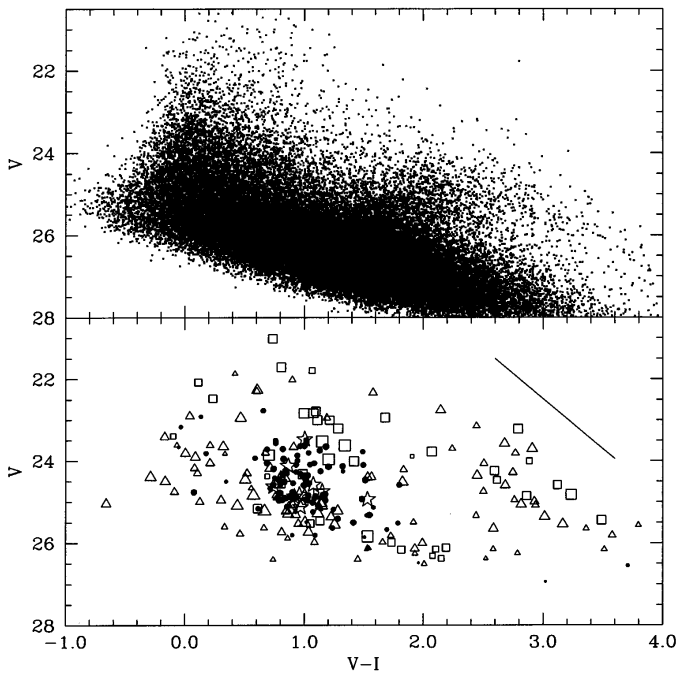

FIG. 4.—Observed color-magnitude diagrams for stars observed in the M101 inner field. The upper panel shows the color-magnitude diagram for nearly 53,000 stars with $\sigma_{V-I} < 0.30$ mag, while the lower panel shows the color magnitude diagram for the 255 variable candidates; symbols are as in Fig. 3. The sloping line shows the effect of interstellar extinction corresponding to $E(V-I) = +1.00$ mag.

ease of finding apparent patterns in small, noisy data sets when many permutations are permitted (i.e., when many periods much shorter than the actual data string are tested).

For our analysis of the PL relation, we have imposed arbitrary period limits of 10 and 48.4 days. The latter, 48.4 days, equals the interval between the first and last V-band observations of the 1994 observing season—as periods progressively longer than this are considered, the template light-curve fits rely more and more heavily on estimating the likely period by matching details of the light-curve morphology, because of the lack of actual repetition of the luminosity variation in the available data set. At the short-period end, the template light curves are calibrated down to a period of 7.0 days, and to this limit there seems to be little danger of confusion between fundamental mode and overtone pulsators. However, careful examination of Figure 3 suggests a fall-off in the mean subjective scores of candidates with magnitudes $V \lesssim 25.5$ mag to 26.0 mag ($I \lesssim$ 24.5 mag to 25.0 mag). Note that $V \sim 26$ mag is also the point where the WS93 index for the sequence of candidate variables tapers down into the main body of stars in Figure 1. This is a result of the fact that near this magnitude the standard error of a magnitude determination becomes comparable to the rms variation in the light curve of a Cepheid. (A particular value of the WS93 index corresponds to a fixed level of statistical significance at all magnitudes, not to a constant amplitude of variation.) It is therefore possible that the faint end of the luminosity function of the shortest period Cepheids may be suppressed by selection effects. To reduce the effect of this bias, we imposed a short-period limit at the slightly larger value of 10.0 days. Apart from this period cutoff, no faint magnitude limit was imposed on the sample to be subjected to further analysis because interstellar extinction is common and can be arbitrarily large. Similarly, no color limit has been imposed since, provided our knowledge of the reddening law is adequate, reddened stars may be included in the analysis.

We remark again that at least some of the stars that lie outside the "Cepheid" region of Figures 3 (the PL relation) and 4 (the color-magnitude diagram) with high objective and subjective quality scores are worthy of further consideration. In particular some of the short-period blue candidates may be main-sequence eclipsing binaries, while some of the stars with very long periods may be $\sim$100 day Cepheids—some of them perhaps highly reddened by the interstellar material associated with their recent births. However, the immediate purpose of the present paper is to estimate the distance to M101 using the Cepheid PL relation, so these potentially fascinating objects will not be considered further here.

The 108 stars within the dashed boundaries in Figure 3 (no selection was made on the basis of position in the color-magnitude diagram) were fitted to the standard Cepheid PL relations

$$M_V = -2.76 \log P - 1.40$$

$$M_I = -3.06 \log P - 1.81$$

derived from Cepheids in the Large Magellanic Cloud by Madore & Freedman (1991). [These zero points assume a true LMC distance modulus $(m - M)_0 = 18.50$ mag and a mean reddening $E(B-V) = 0.10 \Rightarrow E(V-I) = 0.13$.] Stars were all accorded unit weight under the assumption that the width of the intrinsic PL relation and differential reddening completely dominate any purely observational errors, and the resulting apparent distance moduli were $(m - M)_V = 29.49 \pm 0.062$ mag and $(m - M)_I = 29.28 \pm 0.045$ mag [standard errors of the mean, based on 108 stars; these may be compared to the moduli found by Ken98, using a different subsample of Cepheids and mean zero points estimated from a much smaller number of frames: $(m - M)_V = 29.59 \pm 0.06$ mag and $(m - M)_I = 29.43 \pm 0.05$ mag]. Taken together, these imply an average reddening $\langle E(V-I) \rangle = 0.21$ and a true modulus

$$(m - M)_0 = (m - M)_V - A_V = (m - M)_V - 2.45E(V-I) = 28.98 ,$$

where the ratio of total to selective absorption, $A_V = 2.45E(V-I)$ is estimated from the reddening law of Cardelli, Clayton, & Mathis (1989).

However, the statistical uncertainty of this result cannot be determined from simple propagation of errors because both the intrinsic period-luminosity-color relation for Cepheids and interstellar reddening introduce correlations between the V- and I-band residuals; both $\sigma[(m - M)_V]$ and $\sigma[(m - M)_I]$ include the dispersion produced by these two effects, but when the moduli are differenced to remove the reddening, they are almost totally cancelled. Another approach is the standard one adopted in this series of papers: we deredden each star individually, rather than dereddening the sample as a whole. In this case we derive the apparent moduli for each star:

$$(m - M)_V = V + 2.76 \log P + 1.40 ,$$

$$(m - M)_I = I + 3.06 \log P + 1.81 ,$$

and

$$E(V-I) = (m - M)_V - (m - M)_I ,$$

so

$$(m - M)_0 = (m - M)_V - 2.45E(V-I) = 2.45I - 1.45V + 3.50 \log P + 2.40$$

(see Madore 1982). The two formulations are ultimately the same, but with the latter propagation of errors is more straightforward, because the data have been collapsed along the reddening vector, which also coincidentally removes virtually all of the variation due to the finite width of the instability strip.

Crowding and the possible presence of undetected stellar companions—optical neighbors or actual binary companions—can also introduce correlated errors in the V- and I-magnitudes. Contamination is not inherently a well-defined problem. At some level all photometric observations are affected by the presence of astronomical objects other than the target: it is merely a question of whether the relative separation and the magnitude difference between the target and the source of contamination are such as to seriously affect the scientific conclusion. The subject is certainly deserving of further detailed study, but to do it justice would be beyond the scope of the present paper. The following discussion is intended to demonstrate that the effects of contamination by physical companions or chance alignments are not likely to seriously jeopardize our distance estimate for M101.

Of order one-half of all stars in a Population I context are in binaries or multiple systems, and the same statement

appears to be equally valid for Cepheids (see, e.g., Szabados 1992). In the Milky Way, the binary companion of a Cepheid variable is typically a blue main-sequence star, since the luminous red stages of stellar evolution are comparatively brief. Some examples of binary systems consisting of a Cepheid and a red, presumably giant, star are known in the Milky Way, but they are comparatively rare (cf. Table 2 of Szabados 1992). A typical main-sequence companion is less massive, less evolved, and hence less luminous than the Cepheid, especially in the comparatively long wavelengths sampled by the F555W and F814W filters used here. At the distance of M101 or any of the other Key Project galaxies, physically bound systems would be completely unresolved by *HST*, so there would be no hope of visually distinguishing and separating the two components. The joint "bluening" and brightening of the composite spectral-energy distribution is in the same general sense as the reddening vector and is at least partially removed by the dereddening process: projection to the center of the instability strip will sometimes overcorrect for the contamination, sometimes undercorrect, and in the aggregate should have a comparatively small systematic effect. Furthermore, if the population of unrecognized binary companions in the calibrating sample in the LMC is the same as in the target sample, the systematic effect on the inferred distance modulus would tend to zero.

Random alignments of Cepheid variables with comparably luminous field stars in the host galaxy offer another mode of potential contamination. If a Cepheid is blended with a field star that star is bluer than itself, the contamination will be largely removed by the dereddening process, as with a physical main-sequence binary companion. If the Cepheid is blended with a field star redder than itself, on the other hand, the effect is to make the composite brighter and redder—generally orthogonal to the reddening vector—and can introduce a noticeable systematic error in the dereddened true modulus: the presence of the companion makes the variable candidate appear bright, and the redder color of the composite makes it seem reddened, so dereddening the photometry would make the candidate appear brighter still, always producing an anomalously small distance modulus. The scale of this threat is difficult to estimate with great rigor, but it can be crudely estimated from data in hand. In our present sample there are of order 50,000 stars brighter than $V = 27$ mag (which, since our Cepheid sample extends to about $V \sim 26$ mag, is a reasonable guess at the size of the population of objects capable of offering significant contamination). For the sake of an order-of-magnitude estimate, let's say that these objects all fall within the three WFC chips, each of which contains of order 750^2 pixels of effective imaging area. This results in an estimated surface density of roughly one star per 35 pixels. In fact, of order one-half of these stars are bluer than the Cepheids and therefore represent a reduced threat according to the argument outlined above. On the other hand, given that young stars are not uniformly distributed in a galactic disk, it follows that most of them are found in regions of above average density (a tautology). Within the scope of the present discussion we do not have the statistical paraphernalia required to analyze the problem with mathematical rigor, but to continue in the spirit of an order-of-magnitude estimate, let's take these two facts as roughly cancelling each other. If we further assume that, for an optical companion to represent significant contamination, it must lie within a radius of 1–2 pixels of the Cepheid, it follows that somewhere between 1/10 and one-third of Cepheids may be contaminated by an unseen redder optical companion. In fact, we suspect that this is something of an overestimate, at least for the variables with the highest subjective scores, because these will preferentially be Cepheids found in underdense regions, and because an undetected companion of brightness similar to the Cepheid candidate would be revealed as significant fitting residuals in the star-subtracted montage even if the separation were as little as of order 1 pixel. Nevertheless, let us take 1/3–1/10 as our order-of-magnitude estimate of the level of contamination by unseen red optical companions.

From the two preceding paragraphs, we therefore expect that, in spite of the certainty of occasional contamination by physical or optical companions, the bulk (of order 2/3–9/10) of our Cepheids will scatter randomly about the true distance modulus, the uncertainty of which can be inferred from the dispersion of the individual stars about the sample mean. However, a minority, blended with redder field stars of comparable luminosity (not too much brighter, because the variability of the Cepheid would then be imperceptible and the star would not be in the sample; not too much fainter, because then the systematic error would be negligible) will have inferred distance moduli generally smaller than the true value. Finally, the fact that we have preferentially given high subjective scores to variables displaying clean "Cepheid-like" light curves will have further reduced the adverse consequences of Cepheids with unrecognized comparable-brightness companions, though—again—the size of this effect cannot at present be calculated quantitatively. This same conclusion probably applies, within some reasonable range of variation, to Cepheid samples from other external galaxies.

Figure 5 shows, for the 108 plausible Cepheid candidates contained within the dashed boundaries in Figure 3, the individual stars' distance moduli plotted against their combined quality scores (the average of the image and light-

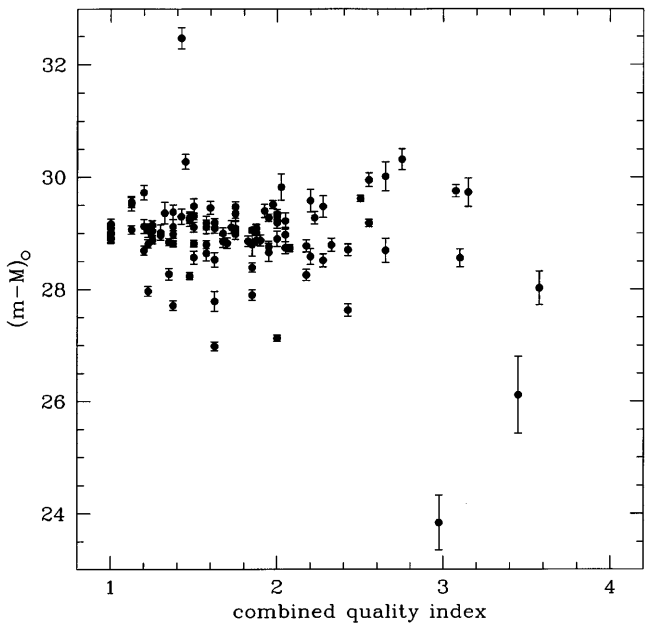

FIG. 5.—Relation between inferred true distance modulus and subjective quality scores for 108 candidate Cepheid variables within the period range 10–48.4 days in the M101 inner field.

curve qualities). The stars with quality scores better (less) than 2.5 cluster strongly near a true modulus of 29.0 mag, with one major outlier at 32.5 mag and a sparse fringe of smaller values. The variables with poorer quality scores include two outliers with moduli <26 mag, but apart from those two, the scatter in true modulus is not really any higher than for the stars with better scores. The main difference is that the Cepheids of "poor" quality have individual error bars nearly commensurate with their scatter, unlike the "good" variables.

Suppose we reject the nine Cepheids with $(m-M)_0 < 28.0$ mag and the four with $(m-M)_0 > 30.0$ mag and average the derived moduli for the remaining candidates with quality indices better than (less than) some cutoff value. Figure 6 illustrates how the mean modulus would vary as a function of the quality-index cutoff. The upper panel shows the variation of the mean apparent V-band modulus as stars of poorer and poorer quality are added to sample, while the second panel shows the corresponding variation in the apparent I-band modulus. It is slightly puzzling that most of the best Cepheids appear to be the ones with the largest apparent moduli; presuming that all are at the same distance, this would mean that for some reason we preferentially give higher scores to more highly reddened Cepheids, or to those on the faint side of the midline of the instability strip. It is conceivable that the subjectively poorer variables are preferentially those projected onto backgrounds that cause us to measure them too bright (stars projected onto holes in the underlying diffuse brightness being more likely to be missed or rejected as too faint). However, this is conjectural and, futhermore, even if this effect is real, it has little effect when the dereddening procedure is applied: the third and fourth panels show the variation in the mean dereddened true modulus and its standard error with sample size, and suggest that the dereddening procedure has largely removed any correlated V- and I-band biases among the poorer quality candidates.

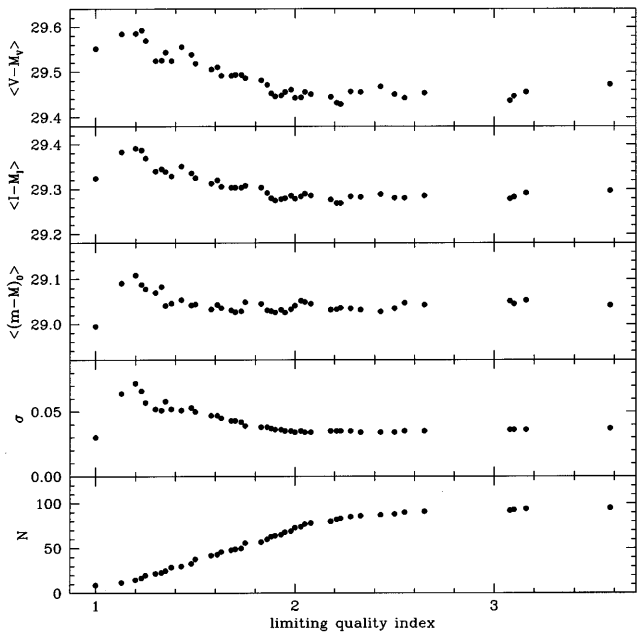

FIG. 6.—Derived distance moduli for all possible subsamples of the 108 Cepheids with $26 < (m-M)_0 < 32$, where the subsamples are defined by $q \le q_{\rm cutoff}$, as a function of $q_{\rm cutoff}$.

The surprise now is that the nine "perfect" variables imply the shortest true modulus of any subsample [they yield $(m-M)_0 = 29.00 \pm 0.030$ mag], while adding in even a few of the barely less-than-perfect variables causes the inferred dereddened modulus to jump abruptly to its maximum value of 29.11 ± 0.072 mag (for the 15 variables with mean quality indices less than 1.20), of course with an accompanying increase in the sample scatter. As more and more of the poorer quality candidates are included, the dereddened true modulus eventually stabilizes near a value of 29.05 mag, and the standard error of the mean true modulus declines roughly as the square root of the number of stars until a limit of 29.04 ± 0.034 mag is reached for the 73 variables with quality scores ≤ 2.0, or 29.04 ± 0.037 mag for the full sample of 95 variables with $28.00 < (m-M)_0 < 30.00$. Thus, it is quite clear that by subjectively choosing the "best" Cepheid variables from among a large sample of candidates, one can arrive at significantly different answers merely by making small changes in the definition of "best" (e.g., by considering the 15 best candidates as compared to the nine best in the present example). Conversely, by making almost no selection at all (e.g., by accepting *all* candidates within a 2 mag band of inferred true modulus), one can—at least sometimes—arrive at an answer well within the range spanned by different plausible samples of "best" Cepheids and a standard error of the mean as good as any that can be derived from more limited samples. This is another way of saying that we do not yet understand how to distinguish objectively good Cepheid variables from poor ones, and that attempts to do so may not always produce a major improvement in the results.

For our final distance modulus for the inner field, we have considered all Cepheid variables meeting the following criteria: (1) variability confirmed by both the ALLFRAME and DoPHOT photometry; (2) a combined image and light-curve quality score <2.0; (3) a period $10.0 < P < 48.4$ days; and (4) an inferred true distance modulus $28.00 < (m-M)_0 < 30.00$ mag (based on the ALLFRAME analysis). All these conditions are met by a total of 61 variables, identified by asterisks in the last column of Table 3. The unweighted arithmetic mean of the ALLFRAME true distance moduli for these 61 stars is $\langle (m-M)_0 \rangle = 29.04 \pm 0.039$ mag [standard error of the mean, standard deviation = 0.30 mag; the two mean apparent moduli are $\langle (m-M)_V \rangle = 29.49$ mag, $\langle (m-M)_I \rangle = 29.31$ mag, so $\langle E(V-I) \rangle = 0.18$]. In comparison, the unweighted mean modulus for the same set of 61 stars based on the periods and mean magnitudes obtained via the DoPHOT analysis is $\langle (m-M)_0 \rangle = 29.05 \pm 0.051$ mag [s.d. = 0.40 mag; $\langle (m-M)_V \rangle = 29.50$ mag, $\langle (m-M)_I \rangle = 29.32$ mag, $\langle E(V-I) \rangle = 0.18$]. Figure 7 plots the dereddened true moduli of these 61 stars against their estimated periods, based on the ALLFRAME analysis. Here the morphology expected from contamination is not particularly apparent: there are three Cepheids of comparatively short period whose low inferred distance moduli might be affected by companions, but if we were to clip the sample symmetrically about the mean, rejecting those stars with $(m-M)_0 < 28.54$ mag and those with $(m-M)_0 > 29.54$ mag, the mean modulus of the remainder would not be significantly different. The *median* modulus among the 61 stars is 29.05 mag, a number that is less precise than the arithmetic mean, but should also be less sensitive to outliers. It appears that there might be some incompleteness at the faintest magnitudes

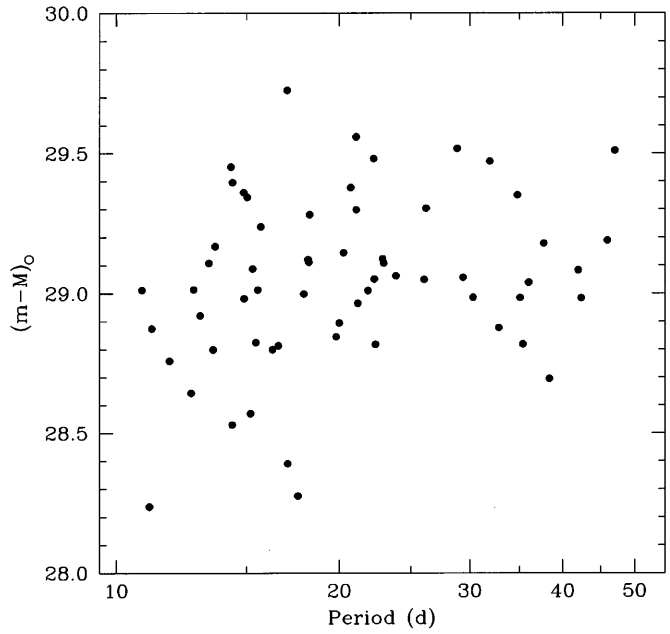

FIG. 7.—Derived true distance modulus vs. period for the 61 Cepheids in the final adopted sample.

for the very shortest periods, in that there are no Cepheids with periods shorter than 11 or 12 days with moduli >29.05 mag or so, where maybe three or four would be expected. However, a close look at the PL relations in Figure 3 reveals a number of candidates plausibly close to the PL relation with periods less than 10 days—the small gap in the faint half of the PL relation at periods of 10–12 days has the appearance of a small-number fluctuation. Nevertheless, if we consider only those 46 Cepheids with periods greater than 15 days, the median dereddened true modulus is still just 29.06 mag, so any putative incompleteness at periods ~ 11 days has no noticeable effect on the final answer.

We therefore adopt an estimated true distance modulus of 29.05 ± 0.05 mag from the M101 inner field data; this value is completely consistent with both the ALLFRAME and DoPHOT photometry, and the error bars embrace both extremes implied by the best ALLFRAME Cepheids: 29.00 mag from the nine best stars, and 29.11 mag from the 15 best. This result may be compared with previous distance estimates found in the literature and presented by Kel96 as their Table 1. The present estimate is rather different from that of Ken98, who estimated $(m - M)_0 = 29.21 \pm 0.09$ mag for the inner field of M101 from a somewhat smaller sample of Cepheids. However, here we have tied the zero points of the V and I magnitude scales to aperture photometry of all observational epochs, while Ken98 tied their zero points to only five exposures, three V and two I, that had the particular virtue of having been taken nearly contemporaneously with similar observations of the outer M101 field. Comparing stars in common to the present study and that of Ken98, we find that the present V-magnitudes average 0.017 ± 0.010 mag (standard error of the mean) fainter, and the I-magnitudes average 0.013 ± 0.007 mag brighter than those of Ken98. Individually, these differences are small, indeed almost negligible, but taken together they mean that the present Cepheid sample is inferred to be some 0.04 mag redder, which would be taken to imply that they are 0.04 mag more heavily reddened, than found by Ken98. When this difference is multiplied by a ratio of total to selective absorption equal to 2.45 and added to the new apparent V-band modulus, it accounts for 0.08 mag of the difference between the true distance moduli from the two studies. The remaining 0.08 mag of the difference must be an artifact of the different Cepheid samples adopted.

It is wisest to rely on the study of Ken98 for the estimate of the dependence of the Cepheid PL relation on metal abundance, because that study was strictly differential: the photometric zero points were determined from nearly contemporaneous WFPC2 exposures for each of the two fields, and the sample of inner-field Cepheids was pruned to match the period distribution available for the outer field. Conversely, the present study and that of Kel96 obtain absolute photometry using the complete set of available data for each field (including the data from the 1995 revisit in the present DAOPHOT study, and a large body of WF/PC data in the previous one). Furthermore, the Ken98 analysis was based on pipeline-calibrated images from STScI and a previous generation of aperture corrections (applied equally to the inner- and outer-field M101 data), whereas the present study utilized reprocessed images from CADC and a new set of aperture corrections based on a much larger body of data. Accordingly, the Cepheid photometry for this study and that of Kel96 are almost completely independent from each other, and largely independent in the sense of both systematic and random errors from the self-contained, differential Ken98 analysis that measured the metallicity dependence of the PL relation. Therefore, if we are to correct the present result for the metallicity difference between the inner M101 field on the one hand and the outer field and the Large Magellanic Cloud on the other, we must add the outer *minus* inner modulus differential of 0.16 ± 0.10 mag found by Ken98 to the M101 inner modulus derived here. The net result is an estimated true distance modulus of 29.21 mag.

The principal elements of the error budget are listed in Table 6. Items (a) and (c) represent the uncertainties of the zero points of the V and I magnitude scales due to the random errors of determining magnitudes in 0".5 apertures either from measurements through smaller apertures plus correction to 0".5, or from profile-fitting photometry plus correction to 0".5 apertures. To arrive at these numbers, the typical uncertainty of a single corrected magnitude (~ 0.03–0.05 mag) can be divided by the square root of the number of stars used to determine it on a given chip (28–50); to the extent that the errors in these corrected magnitudes are random (read noise, photon noise, cosmic rays, warm pixels), the standard deviation can be further divided by the square root of the number of long-exposure frames in each filter ($15V$, $4I$) since it is the effect of these errors on the *mean* zero points that matters; however, to some extent the errors repeat from one epoch to the next (nonuniform sky), so we retain ± 0.01 mag as a conservative estimate of these uncertainties. Even these error estimates, conservative as they are, are dominated by terms (b) and (d), which represent the uncertainties of the zero points of the transformations from true, 0".5 aperture magnitudes to the Landolt (1992) version of the Johnson/Kron-Cousins V, I photometric system. We have assumed a value of ± 0.03 mag for each of these standard errors, which we cannot rigorously justify at the present time, but which we believe to be reasonable. Items [A] and [B] then represent the external

TABLE 6

ERROR BUDGET FOR THE M101 DISTANCE MODULUS

Item	Source of Uncertainty	Individual Uncertainty (mag)	Total Uncertainty (mag)
(a)	$F555W_{0.5}$ aperture correction	± 0.01	
(b)	WFPC2 $F555W_{0.5}$ to V zero point	± 0.03	
[A]	True V-magnitude (a & b)[a]		± 0.032
(c)	$F814W_{0.05}$ aperture correction	± 0.01	
(d)	WFPC2 $F814W_{0.5}$ to I zero point	± 0.03	
[B]	True I magnitude (c & d)[a]		± 0.032
[C]	Mean extinction ($1.45 \times$ A and $2.45 \times$ B)[a]		± 0.09
[D]	ALLFRAME PL fit		± 0.05
[E]	Metallicity		± 0.10
[F]	LMC Distance Modulus		± 0.10
(C & D & E & F)[a]	$(m - M)_0$		± 0.17

[a] All sums are in quadrature.

errors in the zero points of the V and I magnitude systems, which we assume to be independent of one another. These two zero-point uncertainties are amplified by the dereddening process to yield a net systematic error in the zero point of the absolute magnitude system listed as [C]: ± 0.09 mag. The uncertainty that we have inferred from the intrinsic scatter among the derived true moduli of our Cepheids, compounded by the range of possible definitions of an optimum sample, is a minor error contributor at ± 0.05 mag. The two largest sources of uncertainty in the absolute distance of M101 are systematic in nature: the metallicity correction (± 0.10 mag), and the uncertainty in the absolute distance of the Large Magellanic Cloud itself, which, for purposes of the current series of papers, we have taken to be ± 0.10 mag. Our final result, $(m - M)_0 = 29.21 \pm 0.17$ mag, may be compared to the almost completely independent true modulus of 29.34 ± 0.17 mag found for the outer M101 field by Kel96.

6. SUMMARY

We have presented a sample of 255 variable candidates in an inner field of the nearby galaxy M101. Both automatic and subjective methods have been used in an attempt to extract the best possible Cepheids from the total sample, and while no obviously superior selection process has emerged, we find that the true distance modulus estimated for this field does not depend sensitively on the sample selection. The true modulus most probably lies between the values of $(m - M)_0 = 29.00 \pm 0.03$ mag and $(m - M)_0 = 29.11 \pm 0.07$ mag, where these values assume that there is no dependence of the Cepheid PL relation on metallicity, and where the standard errors of the mean are those derived solely from the apparent dispersion among our Cepheids and the adopted sample size. We adopt a "best" uncorrected sample average of $(m - M)_0 = 29.05 \pm 0.05$ mag, where the confidence interval on this quantity has been set to include both of the extreme values given above. Applying a correction of $+0.16$ mag to allow for the abundance difference between the program field and the Large Magellanic Cloud (from the differential analysis of Ken98), and including the remaining contributors to the error budget, we derive a most probable true distance modulus of 29.21 ± 0.17 mag, based on the observations of the M101 inner field. This corresponds to a distance of 7.0 ± 0.6 Mpc. An independent estimate of the true modulus of M101 by Kel96, 29.34 ± 0.17 mag is within one standard deviation of this result. However, because both of these error bars include an allowance of ± 0.10 mag for the true modulus of the LMC, the difference between the estimate and its true standard error are (outer $-$ inner) $= +0.13 \pm 0.20$ mag. An unweighted average of the two moduli is 29.28 ± 0.14 mag (with the uncertainty of the LMC modulus having been subtracted from the uncertainty each of the two estimates and added back in to the uncertainty of the average), implying a distance of 7.2 ± 0.5 Mpc.

We are grateful to the staff of the Canadian Astronomy Data Centre for their continuing excellent service, and to James E. Hesser and the other members of his team for permission to use their data to define our point-spread functions. P. B. S. and S. M. G. H. are grateful to NATO for travel support via Collaborative Research Grant 960178.

REFERENCES

Bresolin, F., Kennicutt, R. C., Jr., & Stetson, P. B. 1996, AJ, 112, 1009
Bresolin, F., et al. 1998, AJ, 116, 119
Cardelli, J. A., Clayton, G. C., & Mathis, J. S. 1989, ApJ, 345, 245
deVaucouleurs, G., deVaucouleurs, A., Corwin, H., Jr., Buta, R., Paturel, G., & Fouqué, P. 1991, Third Reference Catalogue of Bright Galaxies (Berlin: Springer)
Elmegreen, B. G., Elmegreen, D. M., & Montenegro, L. 1992, ApJS, 79, 37
Ferrarese, L., et al. 1998, ApJ, in press
Freedman, W. L., & Madore, B. F. 1990, ApJ, 365, 186
Gilliland, R. L. 1994, ApJ, 435, L63
Hill, R. J., et al. 1998, ApJ, 496, 648
Holtzman, J. A., Burrows, C. J., Casertano, S., Hester, J. J., Trauger, J. T., Watson, A. M., & Worthey, G. 1995, PASP, 107, 1065
Kelson, D. D., et al. 1996, ApJ, 463, 26 (Kel96)
Kennicutt, R. C., Jr., Freedman, W. L., & Mould, J. R. 1995, AJ, 110, 1476
Kennicutt, R. C., Jr., & Garnett, D. R. 1996, ApJ, 456, 504
Kennicutt, R. C., Jr., et al. 1998, ApJ, 498, 181 (Ken98)
Landolt, A. U. 1992, AJ, 104, 340
Madore, B. F. 1982, AJ, 253, 575
Madore, B. F., & Freedman, W. L. 1991, PASP, 103, 933
Moffat, A. F. J. 1969, A&A, 3, 455
Saha, A., Labhardt, L., Schengeler, H., Macchetto, F. D., Panagia, N., Sandage, A., & Tammann, G. A. 1994, ApJ, 425, 14
Saha, A., Sandage, A., Labhardt, L., Tammann, G. A., Macchetto, F. D., & Panagia, N. 1996, ApJ, 466, 55
Sandage, A., & Tammann, G. 1981, Revised Shapley-Ames Catalog of Bright Galaxies (Washington: Carnegie)
Schechter, P. L., Mateo, M., & Saha, A. 1993, PASP, 105, 1342
Scowen, P. A., Dufour, R. J., & Hester, J. J. 1992, AJ, 104, 92
Shields, G. A., & Searle, L. 1978, ApJ, 222, 821
Stetson, P. B. 1987, PASP, 99, 191
———. 1990, PASP, 102, 932
———. 1993, in Calibrating *Hubble Space Telescope*, ed. J. C. Blades & S. Osmer (Baltimore: STScI), 89
———. 1994, PASP, 106, 250
———. 1996, PASP, 108, 851

Stetson, P. B. 1998, PASP, submitted
Stetson, P. B., Davis, L. E., & Crabtree, D. B. 1990, in ASP Conf. Proc. 8, CCDs in Astronomy, ed. G. H. Jacoby (San Francisco: ASP), 289
Stetson, P. B., & Harris, W. E. 1988, AJ, 96, 909
Szabados, L. 1992, in ASP Conf. Proc. 32, Complementary Approaches to Double and Multiple Star Research, ed. H. A. McAlister & W. I. Hartkopf, IAU Colloq. 135 (San Francisco: ASP), 358
Welch, D. L., & Stetson, P. B. 1993, AJ, 105, 1813 (WS93)
Whitmore, B., & Heyer, I. 1997, Instrument Science Report WFPC2 97-08 (Baltimore: STScI)
Zaritsky, D., Elston, R., & Hill, J. M. 1990, in The Interstellar Medium in External Galaxies: Summaries of Contributed Papers (Washington, DC: NASA), 169
Zaritsky, D., Kennicutt, R. C., Jr., & Huchra, J. P. 1994, ApJ, 420, 87